NAVAL POSTGRADUATE SCHOOL
Monterey, California

THESIS

A NUMERICAL MODELING STUDY FOR THE JAPAN/EAST SEA (JES) SEASONAL CIRCULATION AND THERMOHALINE STRUCTURE

by

Hilbert Strauhs

September 1999

Thesis Advisor: Peter Chu
Second Reader: Michael Carron

Approved for public release; distribution is unlimited.

REPORT DOCUMENTATION PAGE

Form Approved OMB No. 0704-0188

1. AGENCY USE ONLY *(Leave blank)*	2. REPORT DATE	3. REPORT TYPE AND DATES COVERED
	September 1999	Master's Thesis

4. TITLE AND SUBTITLE. A Numerical Modeling Study for The Japan/East Sea (JES) Seasonal Circulation and Thermohaline Structure.

5. FUNDING NUMBERS

6. AUTHOR(S)
Hilbert Strauhs

7. PERFORMING ORGANIZATION NAME(S) AND ADDRESS(ES)
Naval Postgraduate School
Monterey, CA 93943-5000

8. PERFORMING ORGANIZATION REPORT NUMBER

9. SPONSORING / MONITORING AGENCY NAME(S) AND ADDRESS(ES)
Naval Oceanographic Office

10. SPONSORING/ MONITORING AGENCY REPORT NUMBER

11. SUPPLEMENTARY NOTES
The views expressed in this thesis are those of the author and do not reflect the official policy or position of the Department of Defense or the U.S. Government.

12a. DISTRIBUTION / AVAILABILITY STATEMENT
Approved for public release; distribution is unlimited.

12b. DISTRIBUTION CODE

13. ABSTRACT ***(maximum 200 words)***

The seasonal sea circulation and thermohaline structure in the Japan/East Sea (JES) were studied numerically using the Princeton Ocean Model (POM) with the horizontal resolution varying from 11.54 to 18.53 km and 15 sigma levels conforming to a relatively realistic bottom topography. A twenty four month control run was performed using climatological monthly mean wind stresses and heat and salt fluxes as surface forcing and observational oceanic inflow/outflow at open boundaries. The seasonally averaged effects of isolated forcing terms are presented and analyzed from the following experiments: 1) non-linear effects removed, 2) no lateral transport at open boundary, and 3) wind effects removed. This procedure allowed analysis of spatial and temporal contributions of the isolated parameter to the general hydrology of the JES and some of its specific features. Major currents are simulated reasonably well compared to the observations. The nonlinear advection does not affect the general circulation pattern evidently, but does affect the formation of the mesoscale eddies, especially the Ulleung Basin (UB) eddy (all seasons) and the Japan Basin (JB) cyclonic gyre (spring). The lateral boundary forcing enhances (weakens) the JES volume transport in the summer (winter). The wind forcing is the most important factor (80 %) for the generation of the JB cyclonic gyre. It drives the Liman Current and damps the East Korean Warm Current in the winter, and generates the UB eddy, and eddies along the Japan Coast Current (JCC) in all seasons. However, it has almost no effect on the JCC for all seasons.

14. SUBJECT TERMS	15. NUMBER OF PAGES
Japan East Sea, numerical simulation, sensitivity studies, circulation, thermohaline structure.	97
	16. PRICE CODE

17. SECURITY CLASSIFICATION OF REPORT	18. SECURITY CLASSIFICATION OF THIS PAGE	19. SECURITY CLASSIFI- CATION OF ABSTRACT	20. LIMITATION OF ABSTRACT
Unclassified	Unclassified	Unclassified	UL

NSN 7540-01-280-5500

Standard Form 298Rev. 2-89)
Prescribed by ANSI Std. 239-18

Approved for public release; distribution is unlimited

A NUMERICAL MODELING STUDY FOR THE JAPAN/EAST SEA (JES) SEASONAL CIRCULATION AND THERMOHALINE STRUCTURE

Hilbert Strauhs
Lieutenant, Brazilian Navy
B.S., Brazilian Naval Academy, 1987

Submitted in partial fulfillment of the
requirements for the degree of

MASTER OF SCIENCE IN PHYSICAL OCEANOGRAPHY

from the

NAVAL POSTGRADUATE SCHOOL
September 1999

Author: 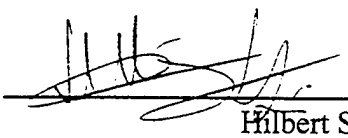
Hilbert Strauhs

Approved by: 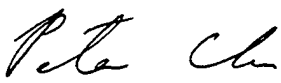
Peter Chu, Thesis Advisor

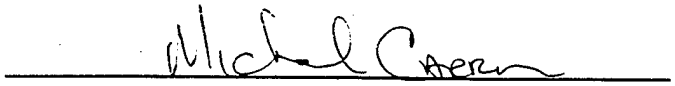
Michael Carron, Second Reader

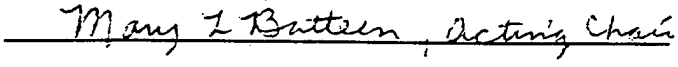
Roland W. Garwood, Jr, Chairman
Department of Oceanography

ABSTRACT

The seasonal sea circulation and thermohaline structure in the Japan/East Sea (JES) were studied numerically using the Princeton Ocean Model (POM) with horizontal resolution varying from 11.54 to 18.53 km and 15 sigma levels conforming to a relatively realistic bottom topography. A twenty four month control run was performed using climatological monthly mean wind stresses and heat and salt fluxes as surface forcing and observational oceanic inflow/outflow at open boundaries. The seasonally averaged effects of isolated forcing terms are presented and analyzed from the following experiments: 1) non-linear effects removed, 2) no lateral transport at open boundary, and 3) wind effects removed. This procedure allowed analysis of spatial and temporal contributions of the isolated parameter to the general hydrology of the JES and some of its specific features. Major currents are simulated reasonably well compared to observations. The nonlinear advection does not affect the general circulation pattern evidently, but does affect the formation of the mesoscale eddies, especially the Ulleung Basin (UB) eddy (all seasons) and the Japan Basin (JB) cyclonic gyre (spring). The lateral boundary forcing enhances (weakens) the JES volume transport in the summer (winter). The wind forcing is the most important factor (80 %) for the generation of the JB cyclonic gyre. It drives the Liman Current and damps the East Korean Warm Current in the winter, and generates the UB eddy, and eddies along the Japan Coast Current (JCC) in all seasons. However, it has almost no effect on the JCC for all seasons.

TABLE OF CONTENTS

LIST OF FIGURES

LIST OF TABLES

ACKNOWLEDGMENTS

I would like to express my appreciation to my advisor, Professor Peter Chu, for his wise guidance throughout the course of my thesis research at the Naval Postgraduate School. Additionally, I would like to thank the Ph.D. student Jose Eduardo Gonçalves for his patient and invaluable help, and the unfailing support of Chenwu Fan, Jian Lan and others in the Naval Ocean Analysis and Prediction Laboratory.

I dedicate this work to Elizabete, my beloved wife, who has survived patiently and endured the last two years as a student at NPS and to my parents Francisco and Ozair who have always been a strong moral support and especially helped us along my wife's pregnancy and delivery of my twin sons Mikael and Nikolas.

I. INTRODUCTION

The Japan Sea, known as the East Sea in Korea, has a steep bottom topography (Fig. 1) that makes it a unique semi-enclosed ocean basin overlaid by a pronounced monsoon surface wind. The Japan/East Sea, hereafter referred to as JES, covers an area of 10^6 km^2. It has a maximum depth in excess of 3,700 m, and is isolated from open oceans except for small (narrow and shallow) straits, which connects the JES to the Pacific Ocean. The JES has great scientific interest as a miniature prototype ocean. Its basin-wide circulation pattern, boundary currents, polar front, mesoscale eddy activities and deep water formation are similar to those in a large ocean.

The JES physical oceanography has been investigated for several decades. The warm Tsushima Current, dominating the surface layer, flows in from the East China Sea through the Tsushima/Korean Strait and carries warm water from the south up to 40°N where a polar front forms (Seung and Yoon, 1995). The cold Liman Current flows in from the Okhotsk Sea through the Tatar Strait and carries cold water from the north. Most of the nearly homogeneous water in the deep part of the basin is called the Japan Sea Proper Water (Moriyasu, 1972) and is of low temperature and low salinity. Above the Proper Water, warm and saline water, which enters through the Tsushima Strait, flows northeastward and flows out through the Tsugaru and Soya Strait.

The seasonal variability of the JES sea surface temperature (SST) has been studied by many investigators (Isoda and Saitoh, 1993; Isoda et al., 1991; Isoda, 1994; Kano, 1980; Maizuru Mar. Observ., 1997) using limited data sets. For example, Isoda and Saitoh (1993) analyzed the satellite infrared (IR) images in the western part of the

JES and the routine hydrographic survey completed by the Korea Fisheries Research and Development Agency in 1987 and found the sea surface temperature (SST) patterns in winter and spring. They found that a small meander of a thermal front originates from the Tsushima Strait near the Korean coast and gradually grows into an isolated warm eddy with a horizontal scale of 100 km. The warm eddy intrudes slowly northward from spring to summer. Recently, Chu et al. (1998a) reported the seasonal occurrence of JES eddies from the composite analysis on the U.S. National Centers for Environmental Prediction (NCEP) monthly SST fields (1981-1994). For example, they identified a warm center appearing in later spring in the East Korean Bay. Chu et al. (1999) further reported the seasonal variation of the thermohaline structure and inverted circulation from the Navy's unclassified Generalized Digital Environmental Model (GDEM) temperature and salinity data on a 0.5° x 0.5° grid.

The JES circulation is extremely complicated owing to its variable and diverse processes such as annual and interannual variations in lateral transport at straits, wind stress, branching of the Tsushima Warm Current (TC), western intensification of the East Korea Warm Current (EKWC), flow separation and eddy shedding and sub-polar front meandering. Present understanding of the circulation in this region is still in the early stage. The recent field observation program on Circulation Research of the East Asian Marginal Seas (CREAMS) (Takematsu et al., 1994; Takematsu et al., 1996) provides information on current variability and water mass distribution for the bottom and intermediate waters.

Recently, Chu et al. (1999) used the Navy's Generalized Digital Environmental Model (GDEM) climatological temperature and salinity data on a 0.5° x 0.5° grid to

investigate the seasonal variabilities of the Japan/East Sea (JES) thermohaline structure and circulations. The GDEM for the JES was built on historical (1930-1997) 136,509 temperature and 52,572 salinity profiles. A three-dimensional estimate of the absolute geostrophic velocity field was obtained from the GDEM temperature and salinity fields using the P-vector method. The climatological mean and seasonal variabilities of the thermohaline structure and the inverted currents such as the Polar Front, the mid-level (50-200 m) salty tongue, the Tsushima Current and its bifurcation, are identified.

Numerical studies on the JES circulations started in early 1980. Various types of models were used such as the multi-layer model (Sekine, 1986, 1991; Kawabe, 1982; Yoon, 1982a,b; Seung and Nam, 1992; Seung and Kim, 1995), the Modular Ocean Model (MOM) (Kim and Yoon, 1994; Holloway et al., 1995; Kim, 1996; and Yoon, 1996; Yoshikawa et al., 1999), the Miami Isopycnal Coordinate Model (MICOM) (Seung and Kim, 1993) and the Princeton Ocean Model (POM) (Chu et al., 1998b, 1999a-g; Guo, 1999; Ro, 1999). Most of the numerical efforts are concentrated on simulating basin-wide circulation, the TC bifurcation, and formation of the intermediate waters. However, there is no modeling study on the formation of the seasonal variabilities of the JES circulation and thermohaline structure.

In this study, we use the Princeton Ocean Model (POM) to investigate mechanisms for the formation of the seasonal variability of the JES circulation and thermohaline structure including the Polar Front meandering and eddies, the TC bifurcation and its effect on the formation of mesoscale eddies in the Ulleung Basin and the Yamato Basin, the Liman Current (LC) and its penetration into the southwestern waters along the Korean coast. The control run, forced by the climatological monthly

wind stress and heat flux, is designed to best simulate reality against which each experiment is compared. In the experiments, various external and internal factors are modified and the resulting circulation patterns and magnitudes compared to the control run results. Specifically, we estimate the contribution, in terms of volume transport and circulation patterns, of non-linear advection, wind forcing and lateral boundary transport to the ocean features identified in the control results. From this, we can estimate the relative importance of these factors to the seasonal variability of the JES circulation and thermohaline structure.

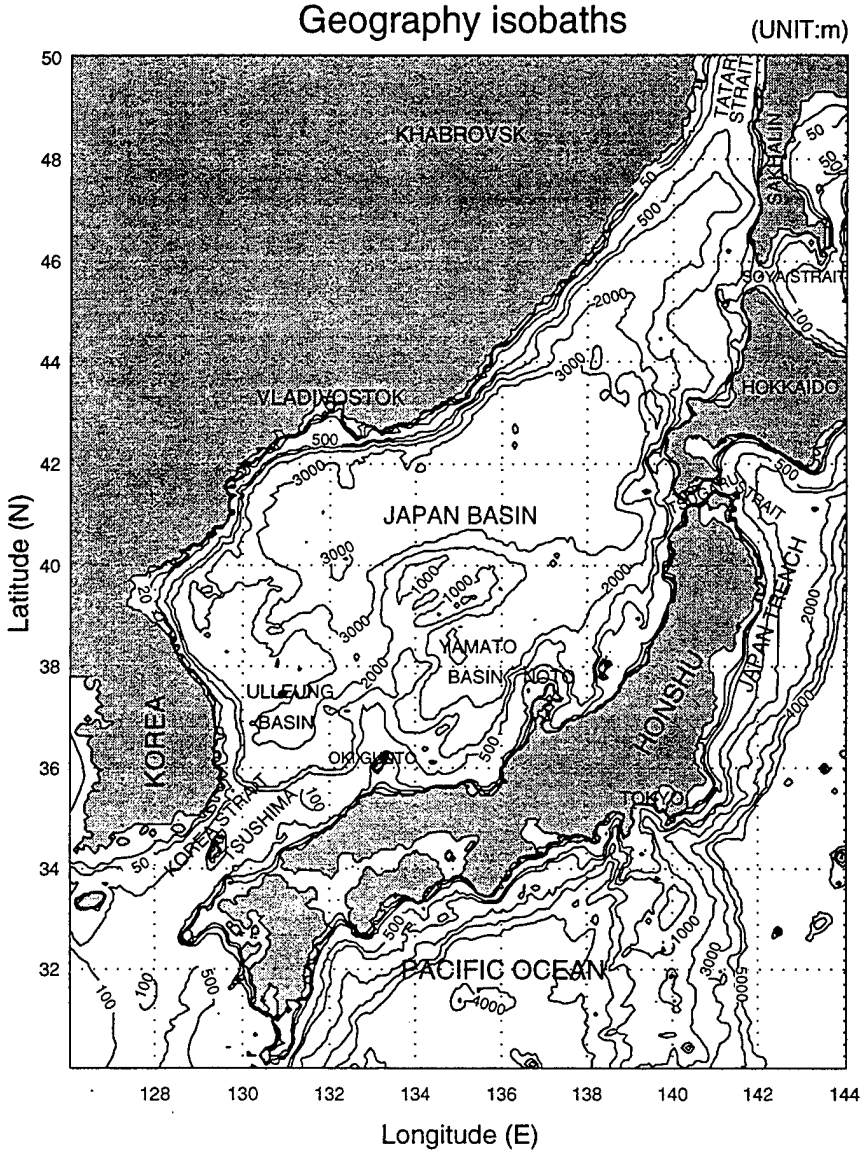

Fig. 1. The Japan East Sea and surrounding areas.

THIS PAGE INTENTIONALLY LEFT BLANK

II. JES CURRENT SYSTEMS

The JES is characterized by a very deep, cold and nearly homogeneous water, the Japan Sea Proper Water which occupies the lower part of the basin (Moriyasu, 1972). The current coming from the East China Sea enters the JES basin through the Tsushima/Korea Straits in the south. The current coming from the Okhotsk Sea enters the JES basin through the Tatar Strait in the north; and the current flows out through the Tsugaru and Soya Straits in the eastern part of JES (Fig. 2).

North of 35°N, the Tsushima Warm Current (TC) separates into two branches into a western and an eastern channel and flows through the western channel, called the East Korea Warm Current (EKWC), and closely follows the Korean coast until it separates near 38°N into two branches. The eastern branch follows the Polar Front to the western coast of Sapporo Island, and the western branch moves northward and forms a cyclonic eddy at the Eastern Korean Bay (EKB). It flows through the eastern channel which closely follows the Japanese Coast, called the Nearshore Branch (NB) by Yoon (1982a, b), or the Japan Coast Current (JCC) by Chu et al. (1999), and it is weaker than through the western channel. The strength of the Tsushima Current at both channels reduces with depth.

The cold water enters the JES from the Okhotsk Sea through the Tatar Strait and forms the Liman Current (LC) or the North Korean Cold Current (NKCC) carrying relatively fresh water along the Russian and North Korean coasts (Seung and Yoon, 1995). The NKCC meets the EKWC at about 37°N with some seasonal meridional migration. After separation from the coast, the NKCC and the EKWC converge to a

strong front that runs in a west-east direction across the basin. The NKCC makes a cyclonic recirculation gyre in the north but most of the EKWC flows out through the outlets (Uda, 1934). The formation of NKCC and separation of EKWC are due to local forcing by wind and buoyancy flux (Seung, 1992). Large meanders develop along the front and are associated with warm and cold eddies.

Seung (1995) identified major features of the volume transport from earlier numerical modeling results. The transport pattern is largely determined by the upper layer circulation and characterized by a large-scale cyclonic recirculation gyre, in which the EKWC and the JCC take part, as the inflow-outflow system, and the NKCC in the North. At a few hundred kilometers off the separation area, the EKWC makes an anticyclonic gyre. The gyre becomes stronger as the EKWC develops. On the other hand, the northern cyclonic gyre is very deep and is most significantly in the winter strengthened by the wind and buoyancy flux. The gyre, or the southward coastal current related to it, is deep enough to intrude southward beneath the EKWC most of the time. Seung also confirmed the summertime presence of counter-current beneath the JCC. North of the Polar Front there exists a cyclonic gyre in the Japan Basin (JB) usually called the JB gyre.

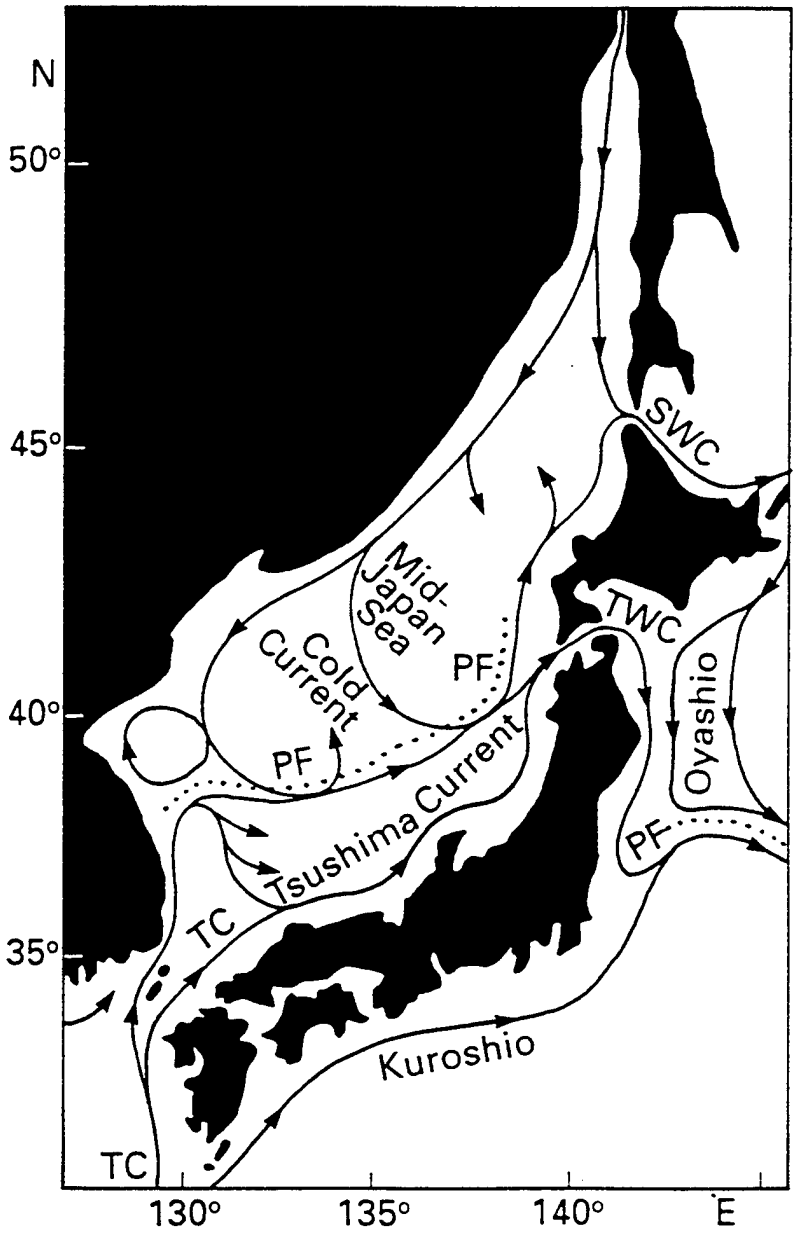

Fig. 2. Surface currents in the JES. EKWC: East Korea Warm Current, PF: Polar Front, SWC: Soya Warm Current, TC: Tsushima Current, TWC: Tsugaru Warm Current. From Tomczak and Godfrey (1994).

THIS PAGE INTENTIONALLY LEFT BLANK

III. SEASONAL VARIATION OF THE ATMOSPHERIC SURFACE FORCING

A. GENERAL DESCRIPTION

The Asian monsoon strongly affects the thermal structure of the JES. During the winter monsoon season, a very cold northwest wind blows over the JES (Fig. 3a) as a result of the Siberian High Pressure System. By late April, numerous frontally-generated events occur making late April and May highly variable in terms of wind speeds and number of clouds. During this period storms originating in Mongolia may cause strong, warm westerlies (Fig. 3b). By late May and early June, the summer surface atmospheric low pressure system begins to form over Asia. Initially this low pressure system is centered north of the Yellow Sea (YS) producing westerly winds. In late June, this low begins to migrate to the west setting up the southwest monsoon that dominates the summer months. The winds remain variable through June until Manchurian low pressure system strengthens. Despite the very active weather systems, the mean surface wind speed over the JES in summer (Fig. 3c) is between 3 and 4 m/s, which is weaker than in winter (Fig. 3a). By July, however, high pressure (the Bonin High) to the south and the low pressure over Manchuria produce southerly winds carrying warm, moist air over the ECS/YS. The summer monthly mean surface air temperature (SAT) is almost the same as the mean sea surface temperature (SST) (Van Loon, 1984). The warm air plus the strong downward net radiation stabilizes the upper layer of the water and causes the surface mixed layer to shoal. October is the beginning of the transition back to winter

conditions. The southerly winds weaken and let the sea surface slope reestablish the winter pattern.

Here, we present a climatological description of the surface net heat and fresh water fluxes over the JES. The datasets used were the objectively analyzed fields of surface marine climatology and anomalies of fluxes of heat, momentum, and fresh water. The fields are derived from individual observations in the Comprehensive Ocean-Atmosphere Data Set (COADS) from 1945 to December 1989 and are analyzed on a 1 by 1 grid (da Silva et al., 1994). The climatological monthly mean values of surface net heat and fresh water fluxes are shown in Figs. 4 and 5.

B. NET SURFACE HEAT FLUX

Net surface heat flux is computed by

$$Q_{Net} = R_S - (R_L + Q_L + Q_S) \quad (1)$$

where R_S is the net downward shortwave radiation, RL the net upward longwave radiation, Q_L the sensible heat flux, and Q_S the latent heat flux. Positive (negative) values of Q_{Net} indicate net heat gain (loss) of the ocean at the surface. The summer field is relatively homogeneous (140-160 W m^{-2}) in the whole JES, whereas a significant horizontal gradient increasing from the southeast (Japan coast) to the northwest (east Russian coast) exists for the rest of the seasons (Fig. 4). The ocean surface near the Tsushima/Korea Strait has the maximum heat loss of 400 W m^{-2} in the winter (January) and the minimum heat gain of 60 W m^{-2} in the spring (April). This long term net surface heat loss will be compensated by the advection of warm waters from the East China Sea.

C. SURFACE FRESH WATER FLUX

The surface fresh water flux is the difference between precipitation rate (P) and evaporation rate (E),

$$F = P - E \tag{2}$$

Positive values of F indicate net water mass gain of the ocean at the surface. The surface fresh water flux exhibits a distinct four-season pattern. The winter is featured by fresh water gain (2-6 cm/month) in the northern and northeastern JES and fresh water loss (2-10 cm/month) in the southern and southwestern JES. A strong horizontal F-gradient is found monotonically decreasing from northeast to southwest. The spring (Fig. 5b) and summer (Fig. 5c) are both characterized by fresh water gain in the whole JES with different horizontal F-gradients: decreasing (increasing) from 4 cm/month (4 cm/month) in the northeast JES to 2 cm/month (6 cm/month) in the southwest JES in the spring (summer). The autumn (Fig. 5d) is featured by fresh water loss in the whole JES (4-16 cm/month) with the maximum loss of 16 cm/month near the Tsushima/Korea Strait.

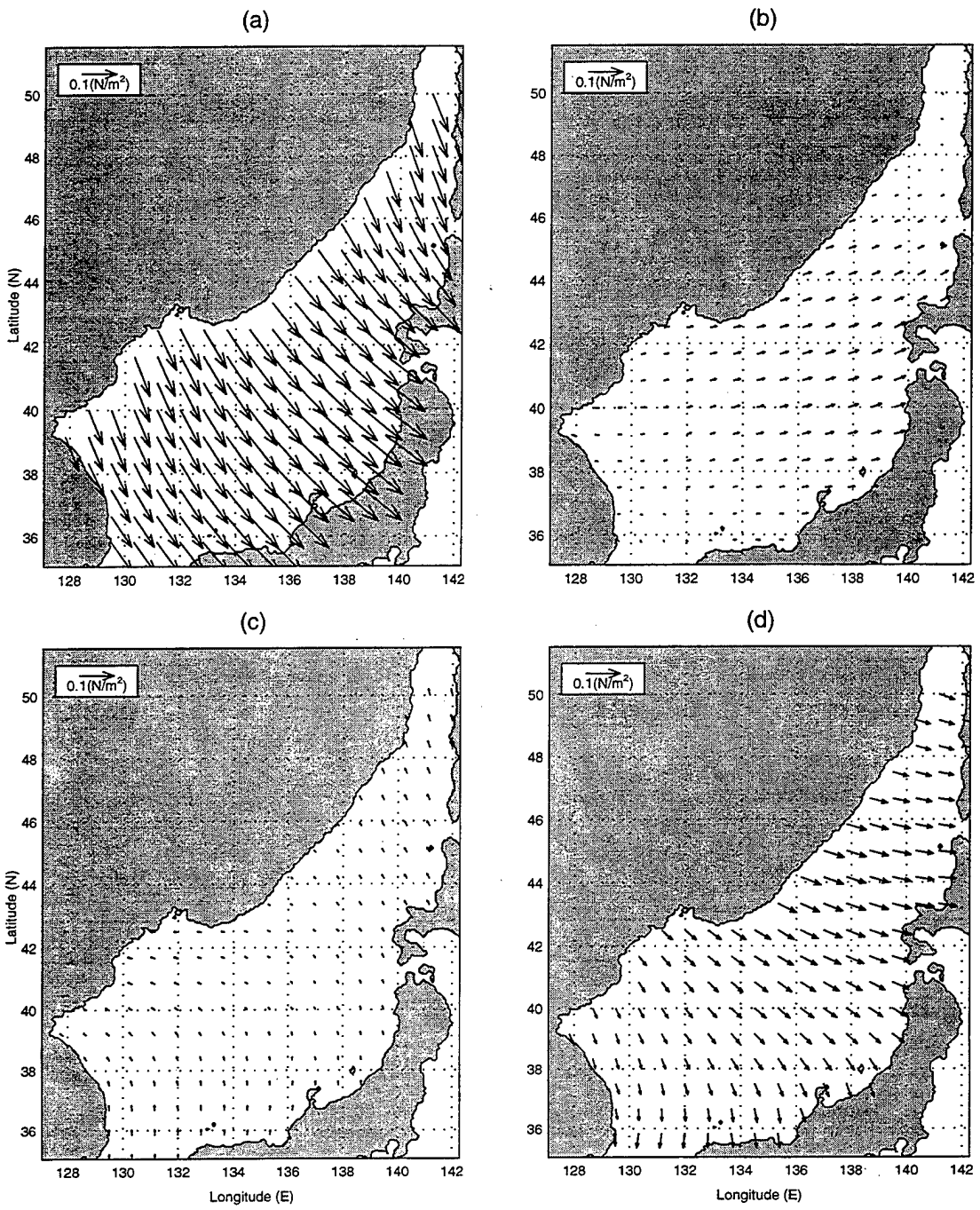

Fig. 3. Climatological wind stress for (a) January, (b) April, (c) July, and (d) October, using the COADS data.

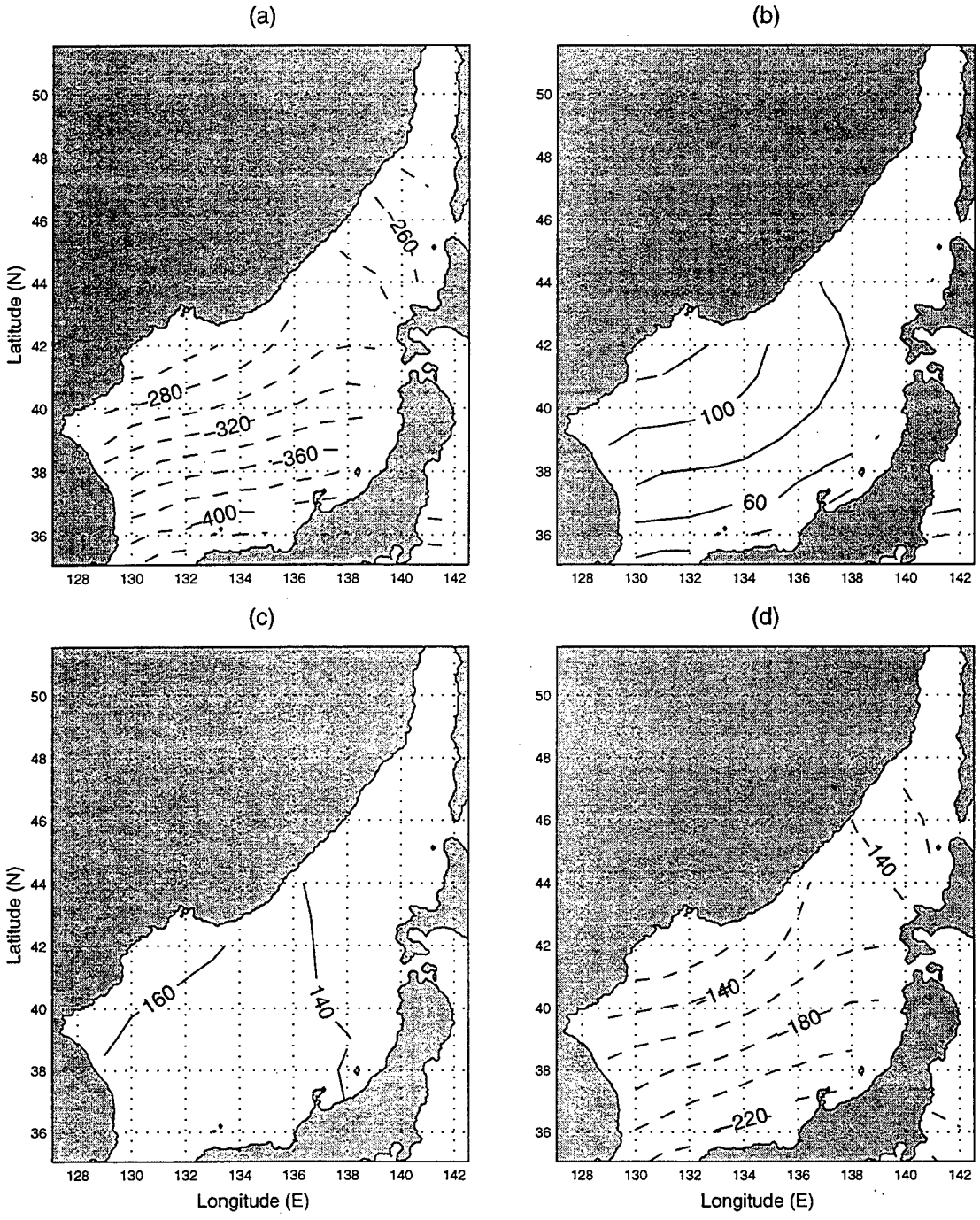

Fig. 4. Net heat (W m^{-2}) for (a) January, (b) April, (c) July, and (d) October, using the COADS data.

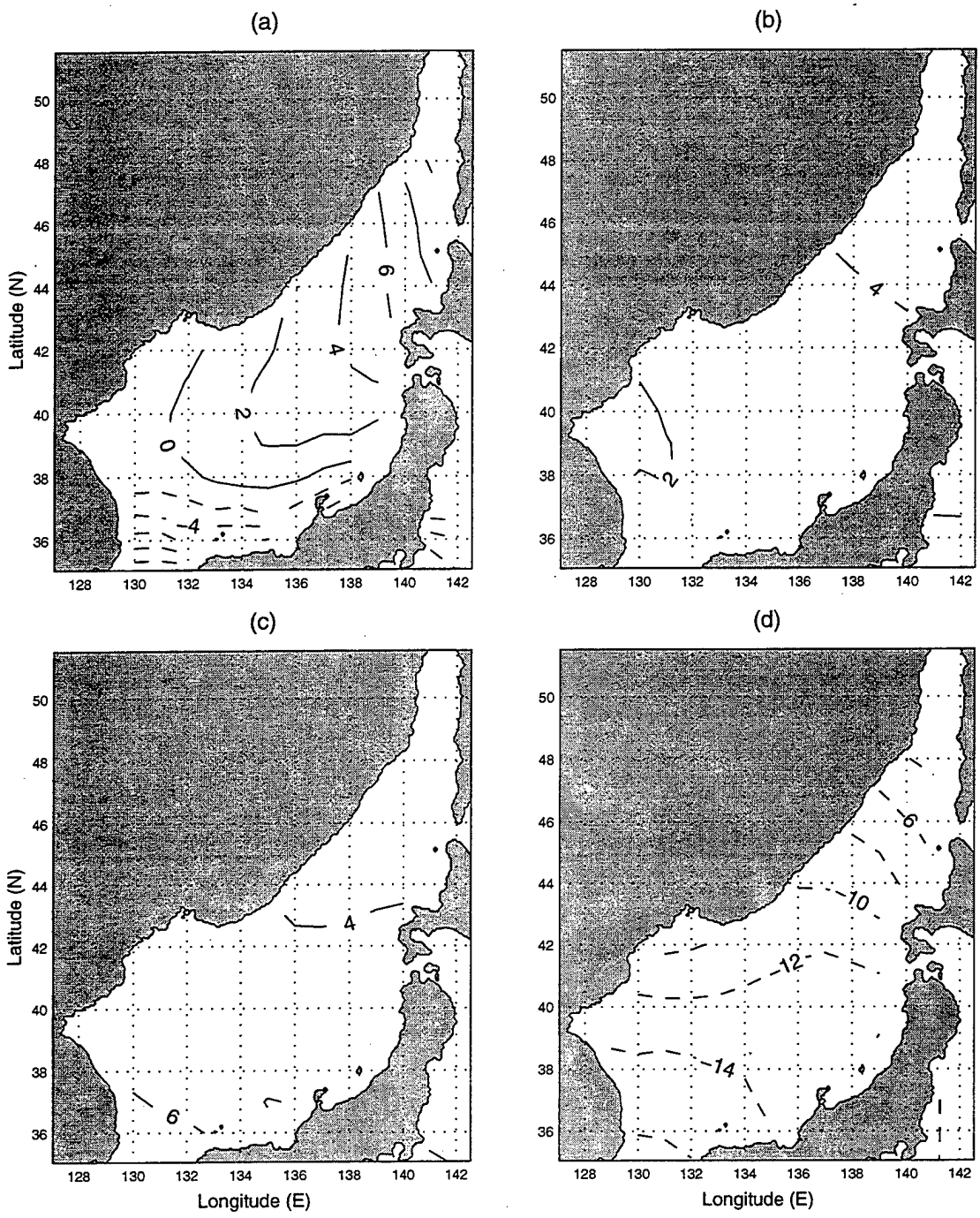

Fig. 5. Precipitation minus evaporation for (a) January, (b) April, (c) July, and (d) October, using the COADS data.

IV. THE NUMERICAL OCEAN MODEL

A. MODEL DESCRIPTION

Coastal oceans and semi-enclosed seas are characterized by extremely high temporal and spatial variability that challenges the existing prognostic capabilities of numerical simulations. The POM is a three-dimensional, free surface, time dependent, primitive equation circulation model on a grid that includes realistic topography (Blumberg and Mellor, 1987). Tidal forcing was not included in this application of the model, since high frequency variability of the circulation is not evaluated. However, the seasonal variations in sea surface height, temperature, salinity, circulation and transport are well represented by the model. From a series of numerical experiments, the qualitative and quantitative effects of non-linearity, wind forcing and lateral boundary transport on the JES are analyzed; yielding considerable insight into the external factors affecting the region oceanography. The model results were sampled every thirty days.

The model contains 94 x 100 x 15 horizontally fixed grid points. The horizontal spacing of 10 minutes (approximately 11.54 to 15.18 km in the zonal direction and 18.53 km in the latitudinal direction) and 15 vertical sigma coordinate levels.

The model domain is from 35.0° N to 51.5° N, and from 127.0° E to 142.5° E. The bottom topography is the smoothed data (Fig. 6) from the Naval Oceanographic Office Digital Bathymetry Data Base 5 minute by 5 minute resolution (DBDB5). The horizontal diffusivities are modeled using the Smagorinsky (1963) form with the coefficient chosen to be 0.2 for this application. The bottom stress τ_b is assumed to follow a quadratic law

$$\tau_b = \rho_0 C_D |\mathbf{V}_b| \mathbf{V}_b \tag{3}$$

where ρ_0 (= 1025 kg/m^3) is the characteristic density of the seawater, $\mathbf{V}_b$ is the horizontal component of the bottom velocity, and C_D is the drag coefficient which is specified as 0.0025 (Blumberg and Mellor, 1987) in our model.

B. ATMOSPHERIC FORCING

The atmospheric forcing for the JES application of the POM includes mechanical and thermohaline forcing. The wind forcing is depicted by

$$\rho_0 K_M \left(\frac{\partial u}{\partial z}, \frac{\partial v}{\partial z} \right)_{z=0} = (\tau_{0x}, \tau_{0y}) \tag{4}$$

where (u, v) and (τ_{0x}, τ_{0y}) are the two components of the water velocity and wind stress vectors, respectively. The wind stress at each time step is interpolated from monthly mean climate wind stress from Comprehensive Ocean-Atmosphere Data Set (COADS), 1945-1989, with the resolution of 1° x 1°. We interpolated the COADS wind stress to the model grid with the resolution of 10'.

Surface thermal forcing is depicted by

$$K_H \frac{\partial \theta}{\partial z} = \alpha_1 \left(\frac{Q_{Net}}{\rho C_p} \right) + \alpha_2 C (\theta_{OBS} - \theta) \tag{5}$$

$$K_S \frac{\partial S}{\partial z} = -\alpha_1 FS + \alpha_2 C (S_{OBS} - S) \tag{6}$$

where θ_{OBS} and S_{OBS} are the observed potential temperature and salinity, and C_P is the specific heat. The relaxation coefficient C is the reciprocal of the restoring time period for a unit volume of water. The parameters (α_1,α_2) are (0,1)-type switches: $\alpha_1 = 1$, $\alpha_2 = 0$, would specify only flux forcing is applied; $\alpha_1 = 0$, $\alpha_2 = 1$, would specify that only

restoring type forcing is applied.

In this study, the surface thermohaline forcing is determined solely by the flux forcing, that is $\alpha_1 = 1$ and $\alpha_2 = 0$ in (5)-(6). The mixing coefficients K_M, K_H, and K_S were computed using a level two-turbulence closure scheme (Mellor and Yamada, 1982).

C. LATERAL BOUNDARY FORCING

Closed lateral boundaries, i.e., the modeled ocean bordered by land, were defined using a free slip condition for velocity and a zero gradient condition for temperature and salinity. No advective or diffusive heat, salt or velocity fluxes occur through these boundaries.

At open boundaries, the numerical grid ends but the fluid motion is unrestricted. Uncertainty at open boundaries makes marginal sea modeling difficult. Three approaches, local-type, inverse-type, and nested basin/coastal modeling, are available for determining the open boundary condition. Here, we take the local-type approach, i.e., to use the radiative boundary condition with specified volume transport. When the water flows into the model domain, temperature and salinity at the open boundary are likewise prescribed from the climatological data (Levitus, 1982). When water flows out of the domain, the radiation condition was applied,

$$\frac{\partial}{\partial t}(\theta, S) + U_n \frac{\partial}{\partial n}(\theta, S) = 0 \tag{7}$$

where the subscript n is the direction normal to the boundary.

Warm water enters the JES through the Tsushima Strait with the Tsushima Current from the East China Sea, and cold water enters the JES through the Tatar Strait with the Liman Current from the Sea of Okhotsk (Tomczak and Godfrey, 1994). The

water exits the JES through the Tsugaru and Soya straits. We found different estimations for the flows through three of the JES straits. It was not an easy job to choose one among them. There is not much information about the transport through the Tatar Strait, which was taken as 0.2 Sv in this study. We use the monthly mean volume transport, reported by Yi (1996), through the Tsushima Strait with the annual average of 1.3 Sv, a maximum of 2.2 Sv in October, and a minimum of 0.3 Sv in February. The total inflow transport through the Tatar and Tsushima straits should be the same as the total outflow transport through the Tsugaru and Soya straits. We assume that 75% of the total inflow transport should flow out of the JES through the Tsugaru Strait, and 25% through the Soya Strait. This ratio is adopted from the maximum volume transport through the Tsugaru Strait estimated by Toba et al. (1982), and through the Soya Strait estimated by Preller and Hogan (1998). The monthly volume transports at open boundaries are listed in Table 1.

Month	Jan.	Feb.	Mar.	Apr.	May	Jun.
Tatar Strait(inflow)	0.2					
Soya Strait (outflow)	-0.32	-0.12	-0.20	-0.15	-0.20	-0.35
Tsugaru Strait(outflow)	-0.68	-0.38	-0.60	-0.45	-0.60	-1.05
Tsushima Strait(inflow)	0.7	0.3	0.6	0.4	0.6	1.2

Month	Jul.	Aug.	Sep.	Oct.	Nov.	Dec.
Tatar Strait(inflow)	0.2					
Soya Strait (outflow)	-0.55	-0.57	-0.57	-0.6	-0.6	-0.4
Tsugaru Strait(outflow)	-1.65	-1.73	-1.73	-1.8	-1.8	-1.2
Tsushima Strait(inflow)	2.0	2.1	2.1	2.2	2.2	1.4

Table 1. The monthly variation of volume transport (1 Sv = 10^6 m^3/s). Here positive (negative) values mean inflow (outflow).

D. INITIAL CONDITIONS AND INITIALIZATION

The model was integrated with all three components of velocity (u, v, w) initially set to zero, and with temperature (Fig. 7) and salinity (Fig. 8) specified by interpolating climatological data (Levitus, 1982) to each model grid point. There is no evident Polar Front identified from this climatological dataset. The model year consists of 360 days

(30 days per month). In order to first capture the winter monsoon, the model was started from day 330 (30 November); day 361 corresponds to 1 December. The control run was integrated from day 330 to day 1440. The sensitivity runs were integrated from day 720's control run results for two years. We use the fourth year's results to compare the JES circulation between the sensitivity and control runs.

E. MODE SPLITTING

For computational efficiency, the mode splitting technique (Blumberg and Mellor, 1987) is applied. The barotropic mode has the time step of 24 sec, based on the Courant-Friederichs-Levy (1928) computational stability (CFL) condition and the external wave speed. The baroclinic mode has a time step of 720 sec, based on the CFL condition and the internal wave speed.

F. EXPERIMENT DESIGN

Our approach was to carry out four numerical experiments: one control and three sensitivity runs. All runs were completed for the same two-year period encompassing both summer and winter monsoons, and, except as specified below, utilized the same initial conditions (on day 331).

Run 1 is the control run. The three sensitivity runs are Run 2, linear dynamics; Run 3, no wind; and Run 4, no lateral transport at the open boundaries. The difference between the control and the sensitivity runs at each grid point and time should then isolate the nonlinear dynamics, lateral boundary effect, and wind forcing effect, allowing independent examination of each.

The thermohaline structure, circulation patterns, and volume transport that constitute the JES oceanography will be identified from the control run for subsequent

comparative analysis. An important assumption is made that the differences are linear, i.e., higher order terms and interactions are negligible and can be ignored. This assumption will be examined and qualified.

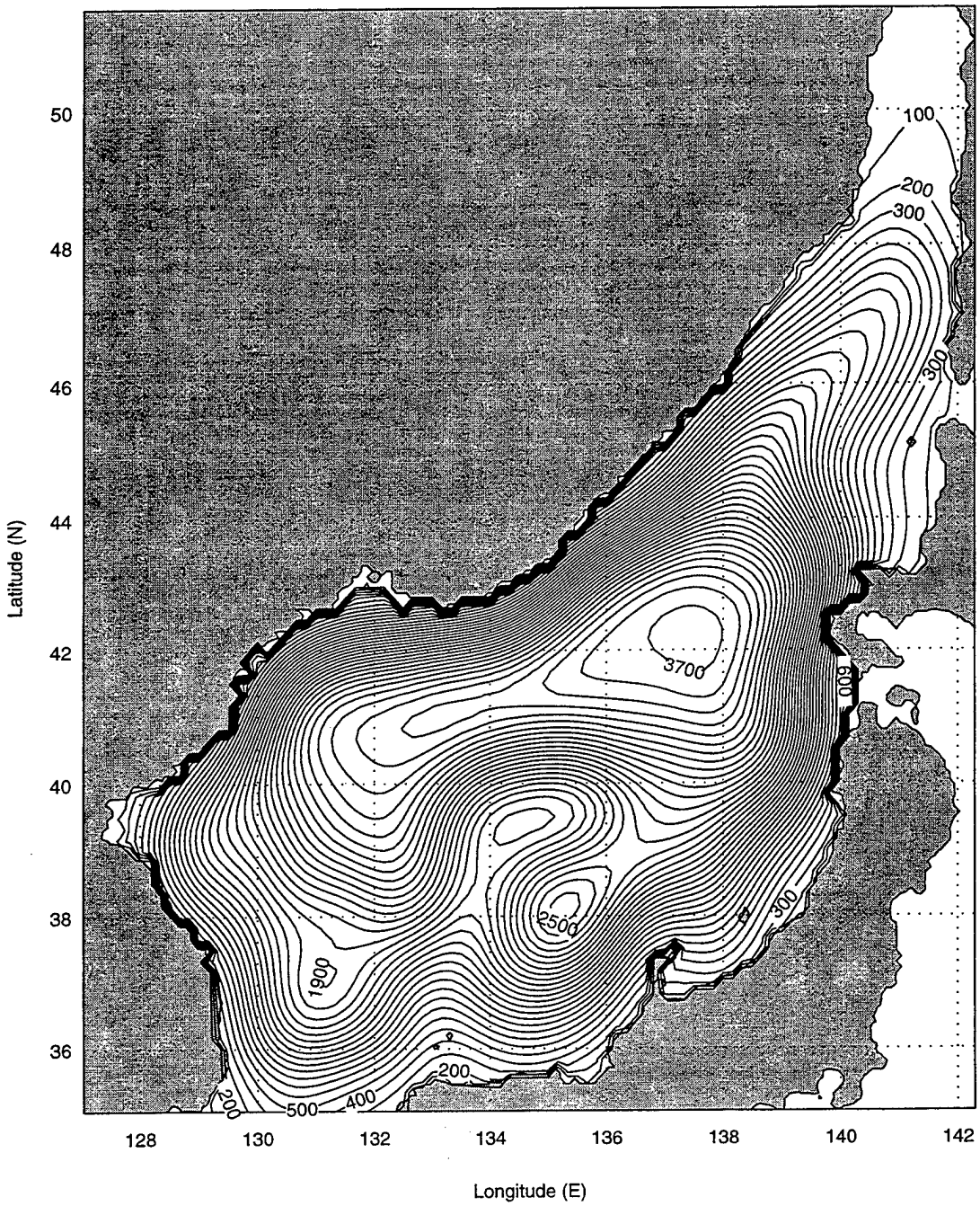

Fig. 6. Smoothed bathymetry.

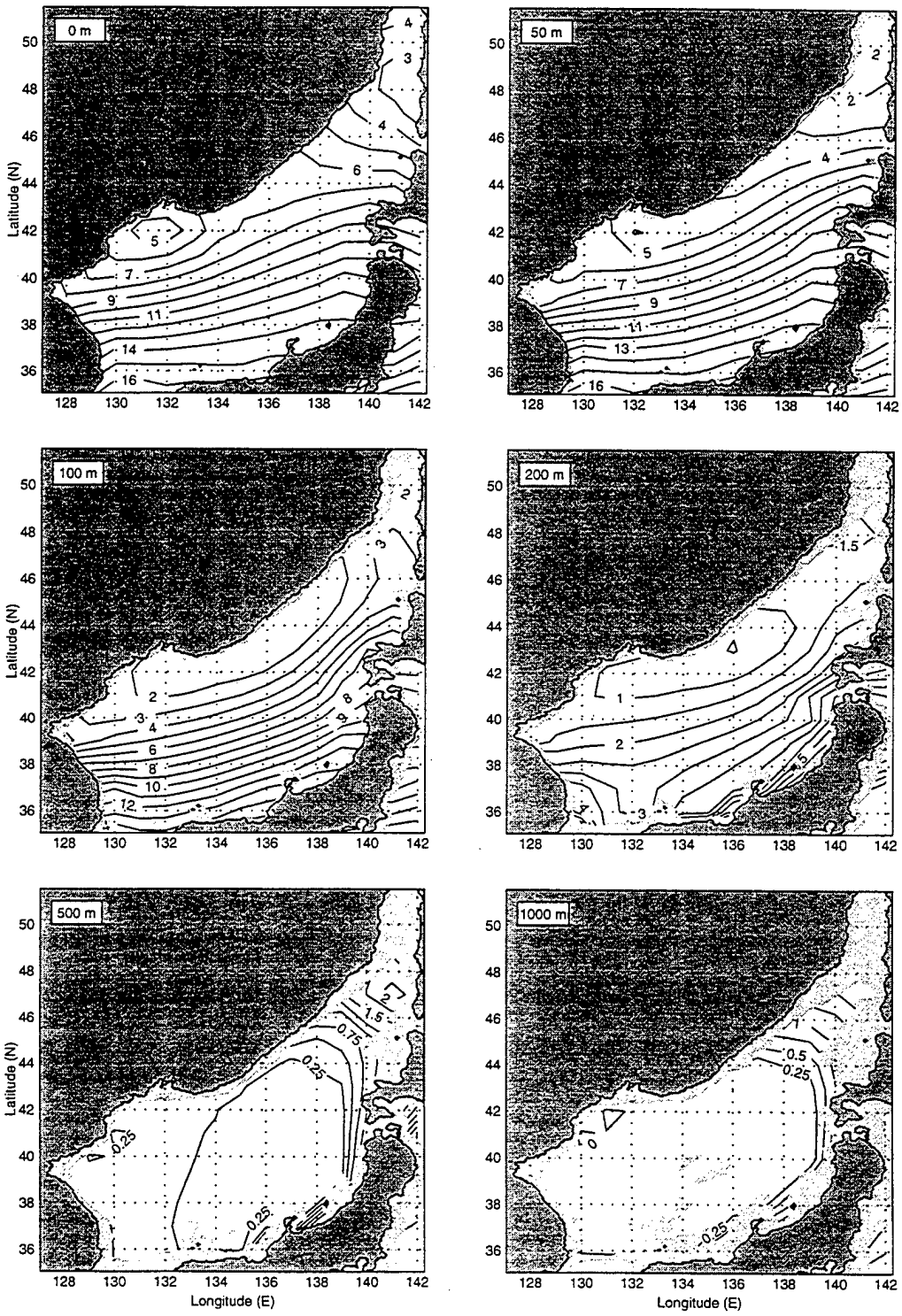

Fig. 7. Initial temperature field (Levitus, 1982) for different depths.

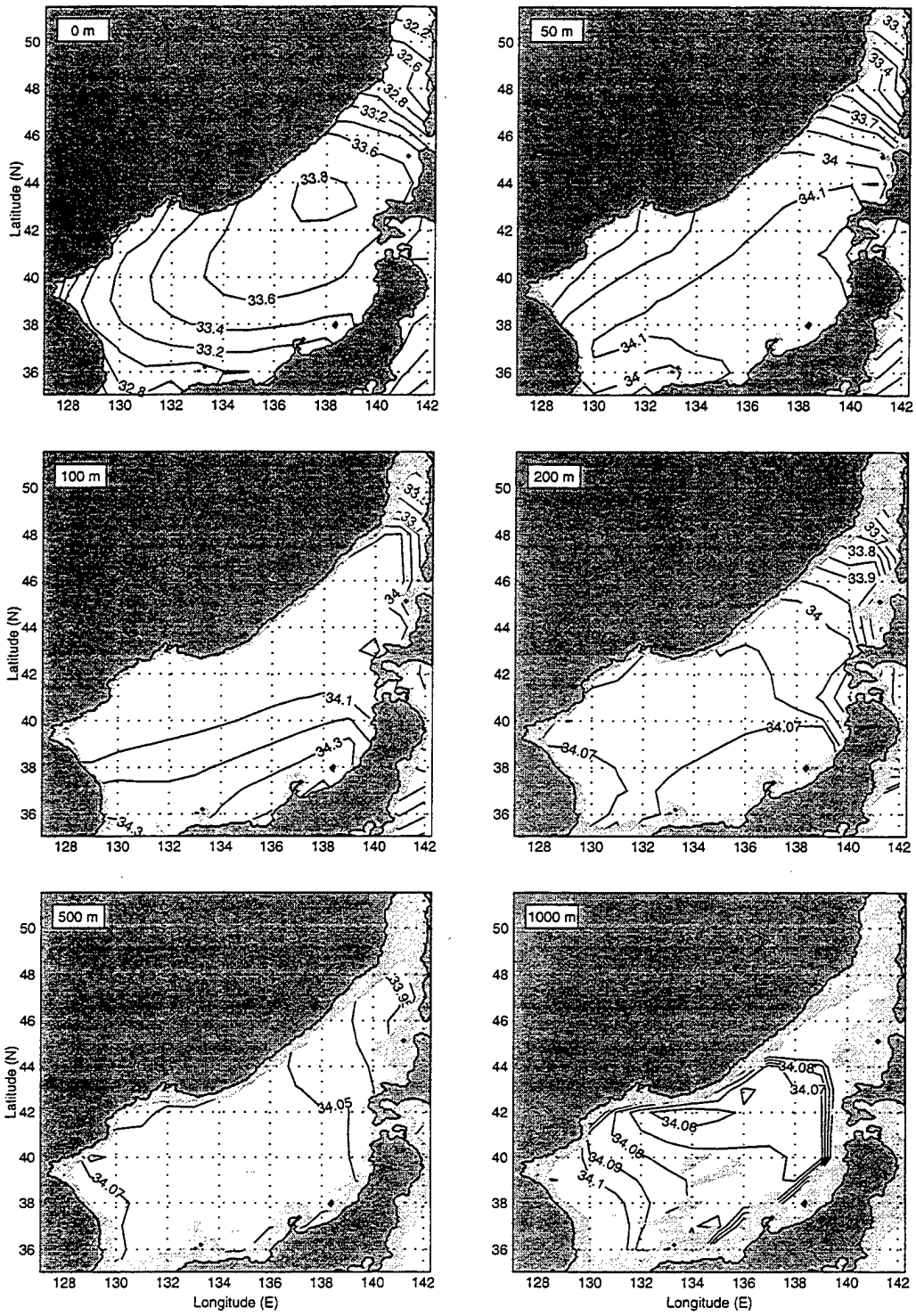

Fig. 8. Initial Salinity field (Levitus, 1982) for different depths.

V. THE SIMULATION (CONTROL RUN)

A. TEMPERATURE

Fig. 9 shows the sea surface temperature (SST) simulated at day-390 (30 January), day-480 (30 April), day-570 (30 July), and day-660 (30 October), respectively. Comparing to the initial temperature field (Fig. 7), the model successfully simulated the formation of the JES Polar Front. Although SST field (Fig. 9) shows an evident seasonal variation, the Polar Front exists at all times throughout the year.

Latitudinal cross-section (135°E) of the temperature field (Figs. 10 and 11) shows a strong north-south thermal asymmetry across the Polar Front. As the depth deeper than 500-m, the temperature is uniformly cold (1-2°C). In the winter (Fig. 10a), the thermocline appears in the southern JES, and disappears north of 41°N. The strength decreases with latitude from 7°C/100m near the Japan coast to less than 1°C/100m at 40°N. From winter to spring (Fig. 10b), the thermocline weakens which however, occurs in the whole JES. We still see the northward decreasing in strength. In the summer, a strong seasonal thermocline, caused by the strong surface heating, is simulated in the shallow depths overlying the permanent thermocline (Fig. 11a). The seasonal thermocline sustains from summer to fall (Fig. 11b). We notice that the simulated vertical gradient of the seasonal thermocline is too large, which indicates that the vertical heat diffusion might not be sufficient in the POM.

B. SALINITY

Three important features are found from the monthly sea surface salinity (SSS) field (Fig. 12): (1) salinity is higher in the winter than in the summer; (2) the seasonal variability of the surface salinity field is stronger in the south than in the north of the Polar Front; and (3) there are two saline activity centers located at the Tatar Strait and the Tsushima Strait, respectively.

Latitudinal cross-sections (135°E) of salinity show a strong north-south haline asymmetry across the Polar Front (Figs. 13 and 14): mid-level (200-500 m) salty tongue (34.1 psu) appears south of the Polar Front and disappears north of the Polar Front. The shallow and strong halocline associated with strong thermocline makes the sub-surface water mass north of the Polar Front hydrostatically stable. The mid-level salty tongue associated with weak and wide thermocline makes the water mass hydrostatically less stable south of the Polar Front.

C. CIRCULATION

Fig. 15 shows the sea surface velocity vectors simulated at day-1140 (30 January, winter), day-1230 (30 April, spring), day-1320 (30 July, summer), and day-1410 (30 October, fall), respectively. The simulated surface velocity field (Fig. 15) coincides with the earlier description of the JES circulation presented in Chapter 2. The TC separates at the Tsushima/Korea Strait into two branches into a western and an eastern channel. Flow through the western channel (i.e., EKWC) closely follows the Korean coast until it separates near 38°N into two branches. The eastern branch follows the Polar Front to the western coast of Sapporo Island, and the western branch, moves northward and forms a cyclonic eddy at the Eastern Korean Bay (EKB). Flow through the eastern channel (i.e.,

JCC) is a little weaker than through the western channel. The LC carries fresh and cold water along the Russian coast and becomes the NKCC at the North Korean coast. The simulated NKCC meets the EKWC at about 38°. After separation from the coast, the NKCC and the EKWC converge to a strong front that runs in the west-east direction across the basin. The seasonal variation of the JES circulation is also simulated.

To investigate the JES circulation as a whole, we integrate the velocity vertically from the surface (z = 0) to the bottom (z = -h)

$$U = \int_{-h}^{\eta} u dz, \quad V = \int_{-h}^{\eta} v dz \tag{8}$$

Due to the continuity the volume transport stream function (P) is defined by

$$U = -\frac{\partial \psi}{\partial y}, \quad V = \frac{\partial \psi}{\partial x} \tag{9}$$

and satisfies the Poisson equation

$$\nabla^2 \psi = \frac{\partial V}{\partial x} - \frac{\partial U}{\partial y} \tag{10}$$

For each time instance, we solve the two-dimensional Poisson equation (10) with the given boundary conditions, that is, zero transport at the rigid boundaries and known transport at the open boundaries (see Table 1).

Fig. 16 shows the contour plots of the volume transport stream function simulated at day-1140 (30 January, winter), day-1230 (30 April, spring), day-1320 (30 July, summer), and day-1410 (30 October, fall), respectively. The unit is in Sv (1 Sv = 10^6

m^3/s). The volume transport moves with the smaller values on the left. The strength of the transport is evaluated by the difference between two contours. The northern JES is occupied by a cyclonic gyre (called the JB gyre) and the southern JES is characterized as a multi-eddy structure. The volume transport streamfunction (Ψ) has a double-gyre structure with negative values (cyclonic) in the northern JES and positive values (anticyclonic) in the southern JES. It has an evident seasonal variation with the appearance of the cyclonic gyre in the northern JES (i.e., the JB) in the winter and spring and disappears in the summer and fall.

1. Japan Basin (JB) Cyclonic Gyre

A large-scale cyclonic recirculation gyre over the JB is simulated with a strong seasonal variation. This gyre is easily identified by the volume transport streamfunction (Fig. 16). The JB gyre is the strongest and recirculates 8 Sv in the winter. It weakens and retreats northward in the spring and summer. In the fall, the cyclonic JB gyre disappears and weak anticyclonic eddies appears. Our simulation is consistent with the earlier study (Seung and Yoon, 1995).

2. Liman Current (LC)

The LC is a southwestward current following along the Russian coast. It bifurcates into two branches near the east Russian bight (134°E, 42°N): the western branch flows along the Russian-Korean coast and becomes the NKCC. The eastern branch flows southeastward, then turns eastward at 41.5°N, and becomes the south frank of the Japan Basin (JB) gyre. The LC has a strong seasonal variation with the maximum speed in the winter (Fig. 15a) and the minimum speed in the summer (Fig. 15c).

Zonal cross-sections of the v-velocity at 46°N for four different seasons indicate seasonal and spatial variabilities of the LC. It has a maximum southward component (0.21 m/s), occurring near the surface in winter (Fig. 17b) with the width of 100 km and the depth of 800 m. The core of the LC is close to the coast and near the surface. In the spring, its strength weakens to 0.18 m/s (Fig. 18), but the width and depth keep almost unchanged. It further weakens to a minimum of 0.15 m/s in the summer (Fig. 19b) and in the fall (Fig. 20b), and shrinks its size into a width of 60 km and depth of 400 m.

3. East Korean Warm Current (EKWC)

EKWC, western branch of TC north of the Tsushima/Korea Strait, acts as a western boundary current and has a strong seasonal variability. At 37°N, the EKWC v-velocity component, which is practically the direction of the current on that position, varies from 0.42 m/s in summer (Fig. 21a), to 0.30 m/s in winter (Fig. 22a). The width of EKWC is around 60 km all year round. However, the depth is around 1,400 m in the summer and 800 m in the winter.

4. EKWC – NKCC Confluence

The (northward) overshooting of the EKWC near the Korean Bight at 37.5° N is stronger in the winter than in the summer (Fig. 15). The overshot EKWC leaves the Korean coast and moves northward. It converges with the southward flowing NKCC, at 39°N, 130°E, and forms a current meandering toward the east along the Polar Front, defined as the Polar Front Current (PFC) by Chu et al. (1999). The resultant velocity of the PFC is 0.32 m/s and northeastward, in the fall (Figs. 20a and 23a), and 0.21 m/s in the winter (Figs. 17a and 24a).

5. Japan Coastal Current (JCC)

JCC, the eastern branch of TC north of the Tsushima/Korea Strait at 132°E, has a maximum eastward component of 0.24 m/s in the winter (Fig. 25a). A counter current beneath it is simulated with a westward component of 0.12 m/s. In the summer, the counter current remains almost unchanged, but the JCC falls down to 0.09 m/s (Fig. 26a). Seung and Yoon (1995) observed the counter current in the summer. However, we simulated the counter current all year round.

The effect of coastal geometry, such as the Noto Peninsula, on the JCC is also simulated. The JCC current turns its direction from the eastward to north-to-northeastward along the Noto Peninsula (Fig. 15). The inflow from the Tsushima/Korean Strait has a strong seasonal variation with the maximum transport in the fall and the minimum transport in the spring (Table 1). The v-component near the tip of the Noto Peninsula should have a corresponding variation. Such a topographic steering is clearly seen from the zonal cross section of the v-component at 37°N. The northward component has a maximum (minimum) value of 0.21 (0.15) m/s in fall (spring) near 137°E, as shown in Fig. 27. Furthermore, the north-to-northeastward JCC near the Noto Peninsula is quite narrow and shallow. The width is around 50 km, and the depth is nearly 300 m. Away from the narrow JCC, there exists a counter current further off shore and an undercurrent, both southward. These currents are weak in the spring (0.06 m/s) and become evident (0.09 m/s) in the fall.

6. Ulleung Basin (UB) Eddy

The western branch of the warm TC (i.e., EKWC) moves northward along the southern part of Korean coast and separates from the coast after approaching the East

Korean Bay (EKB). It keeps its northward motion until meeting the NKCC near 40°N, meanders southeastward, and forms a warm-core anticyclonic eddy (Fig. 15). The simulated anticyclonic UB eddy is strongest in the summer (Fig. 15c). The center is located at 38.5°N 130°E. The size of the eddy is around 150 km. The tangential velocity is around 0.4 m/s.

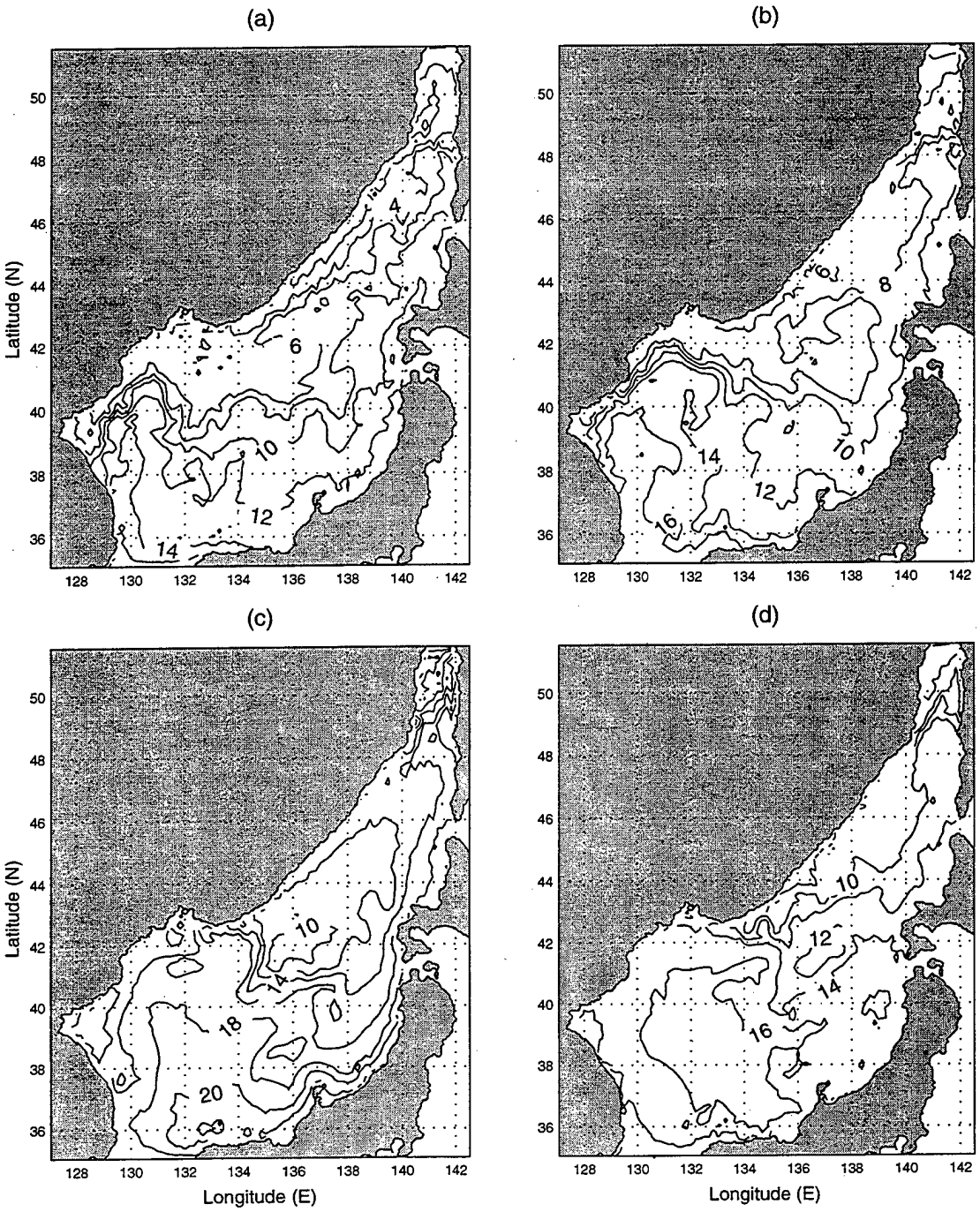

Fig. 9. Temperature (°C) field results from first year of run for (a) January, (b), April (c), July and (d) October.

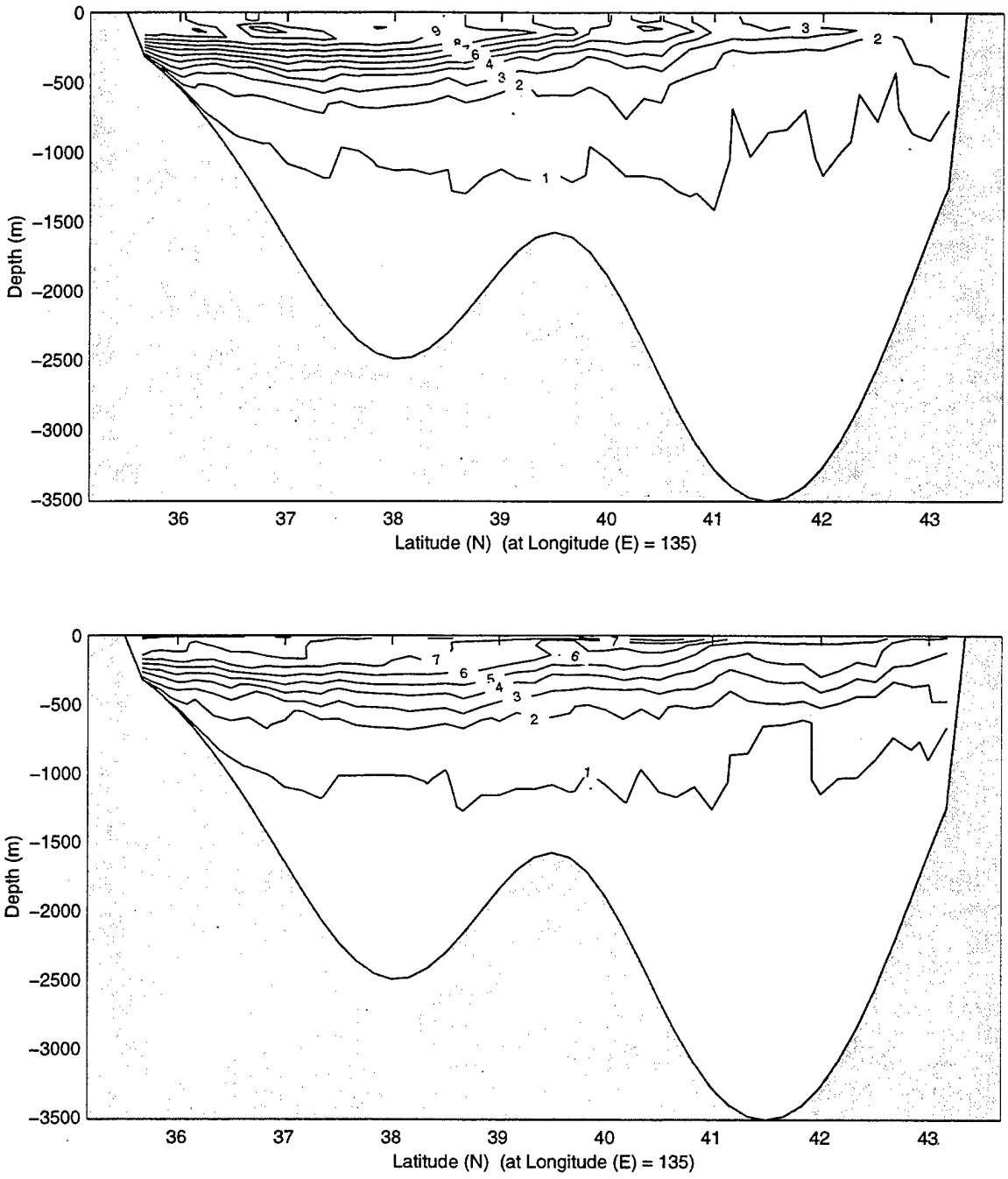

Fig. 10. Temperature (° C) results from first year on cross-sections at 135° E for (a) January and (b) April.

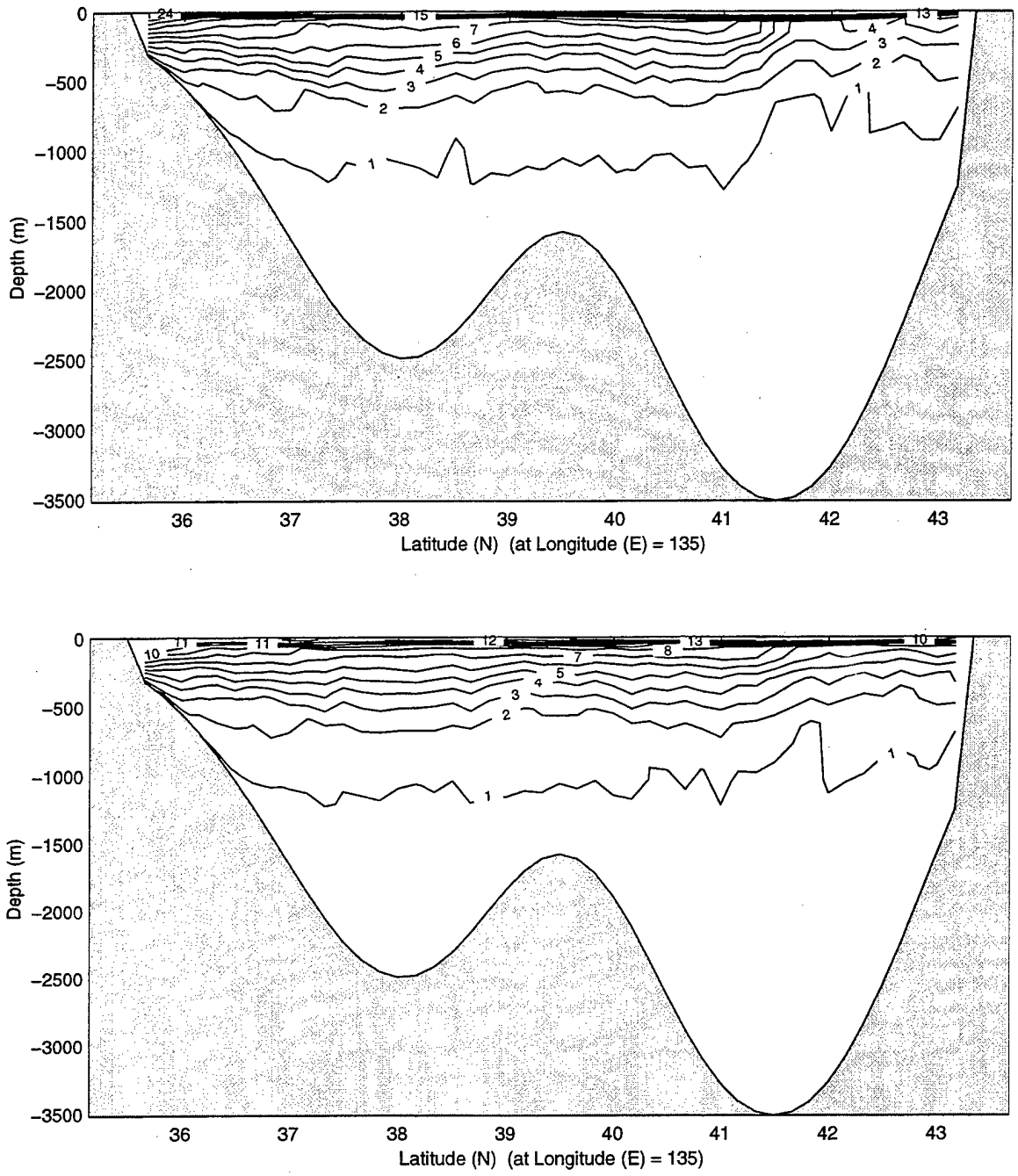

Fig. 11. Temperature (° C) results from first year on cross-sections at 135° E for (a) July and (b) October.

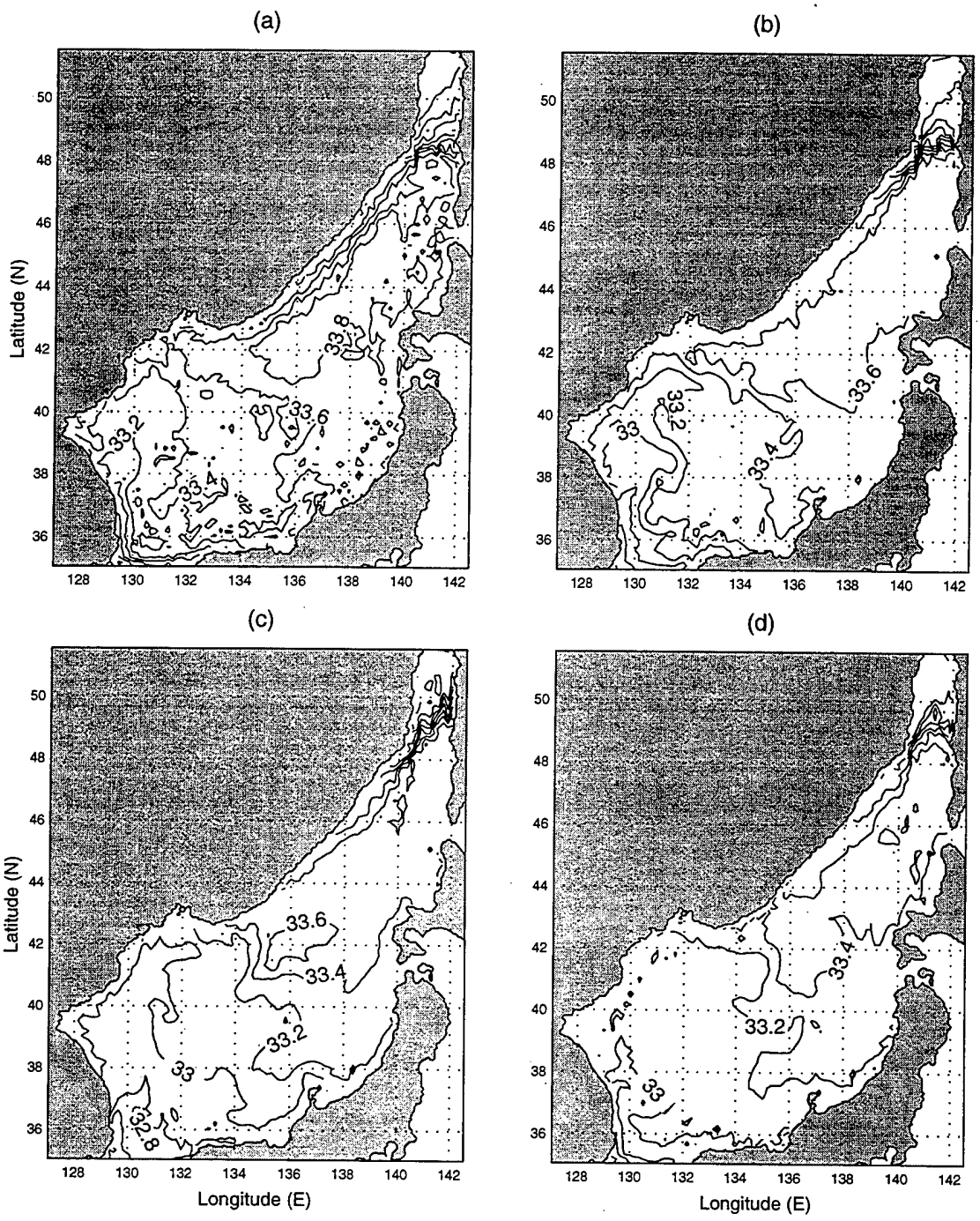

Fig. 12. Surface salinity field from the first year results for (a) January, (b) April, (c) July and (d) October.

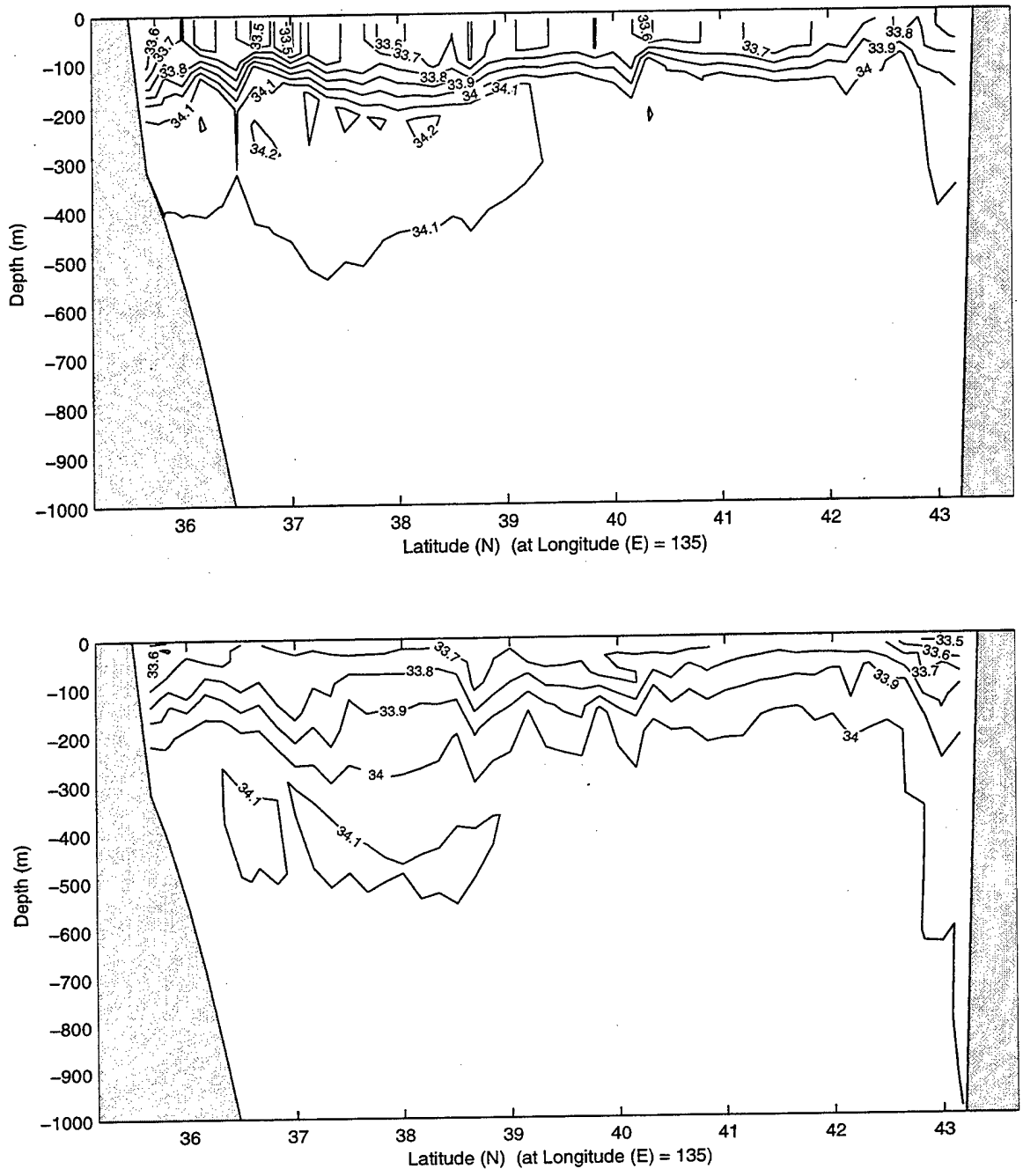

Fig. 13. Salinity (psu) results from first year on cross-sections at 135° E for (a) January and (b) April.

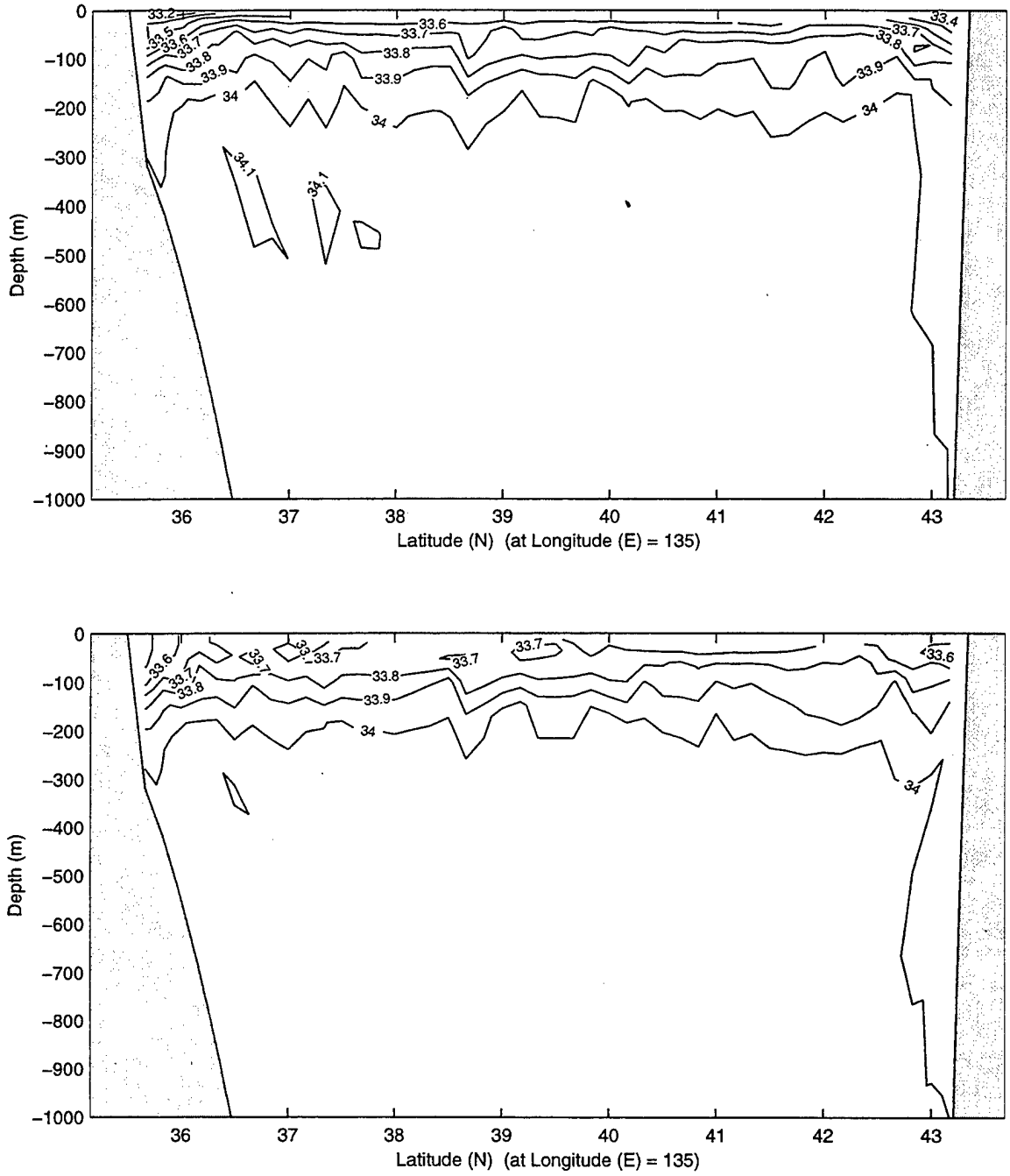

Fig. 14. Salinity (psu) results from first year on cross-sections at 135° E for (a) July and (b) October.

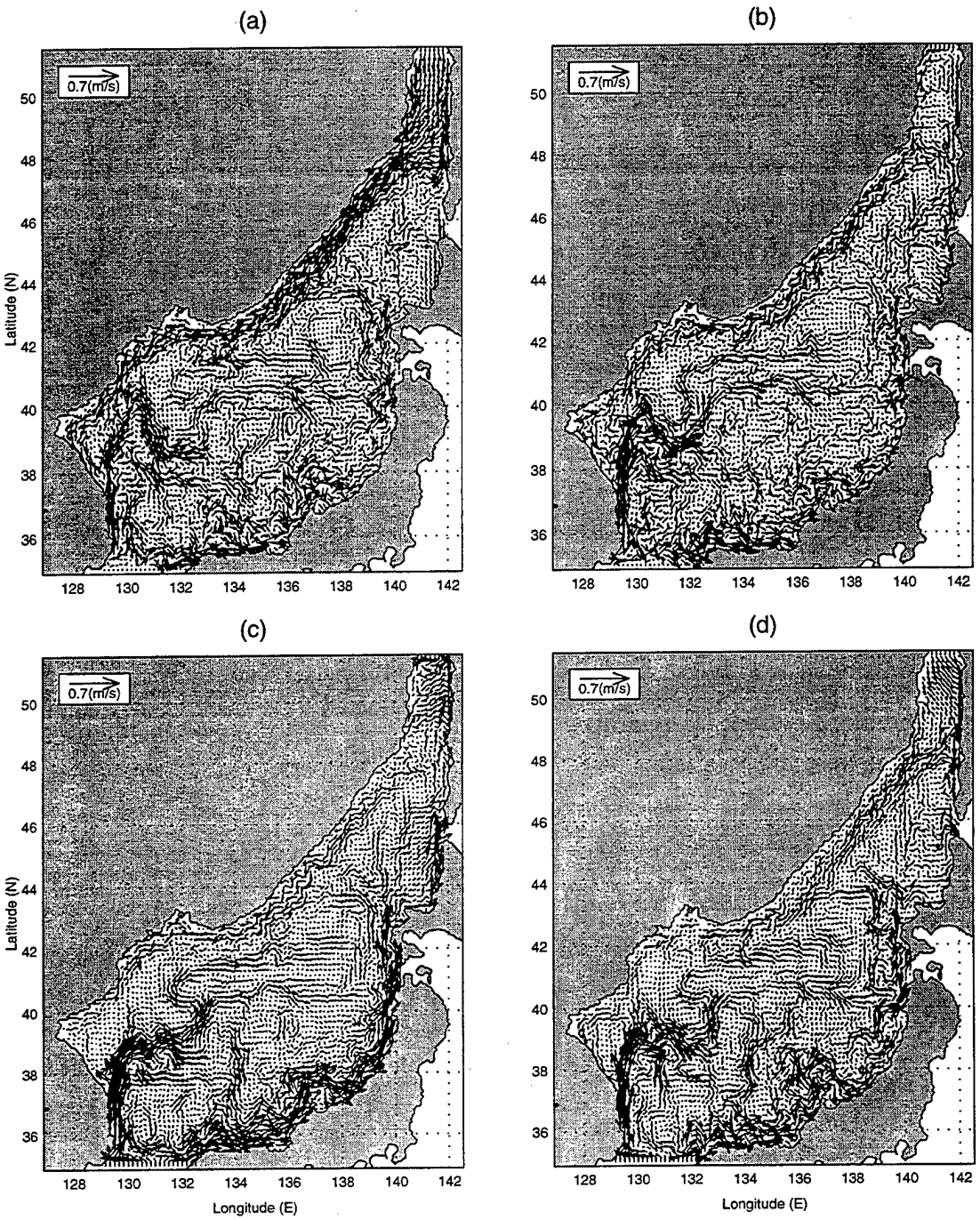

Fig. 15. Surface circulation from control run for (a) January, (b) April, (c) July and (d) October.

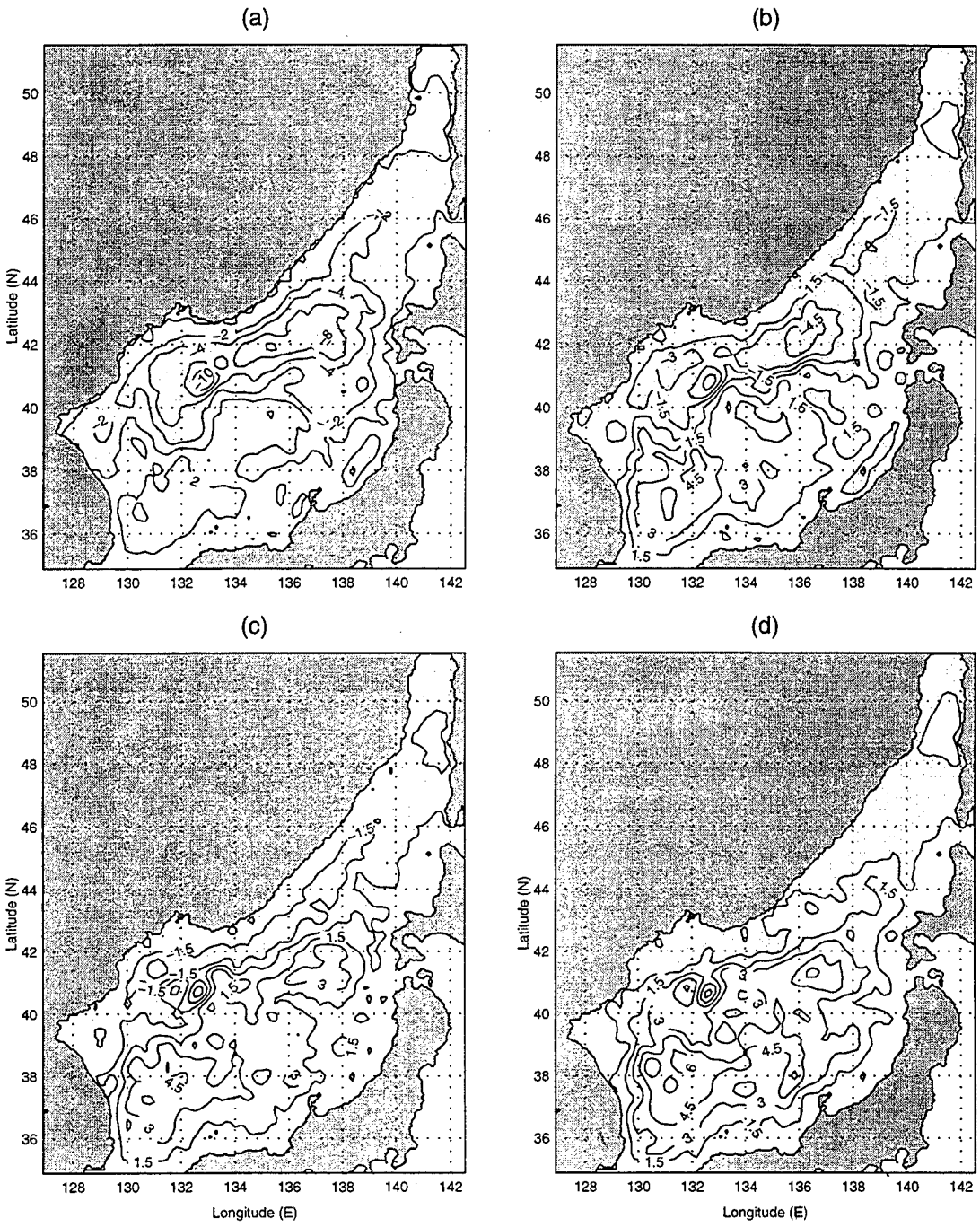

Fig. 16. Volume transport for (a) January, (b) April, (c) July and (d) October.

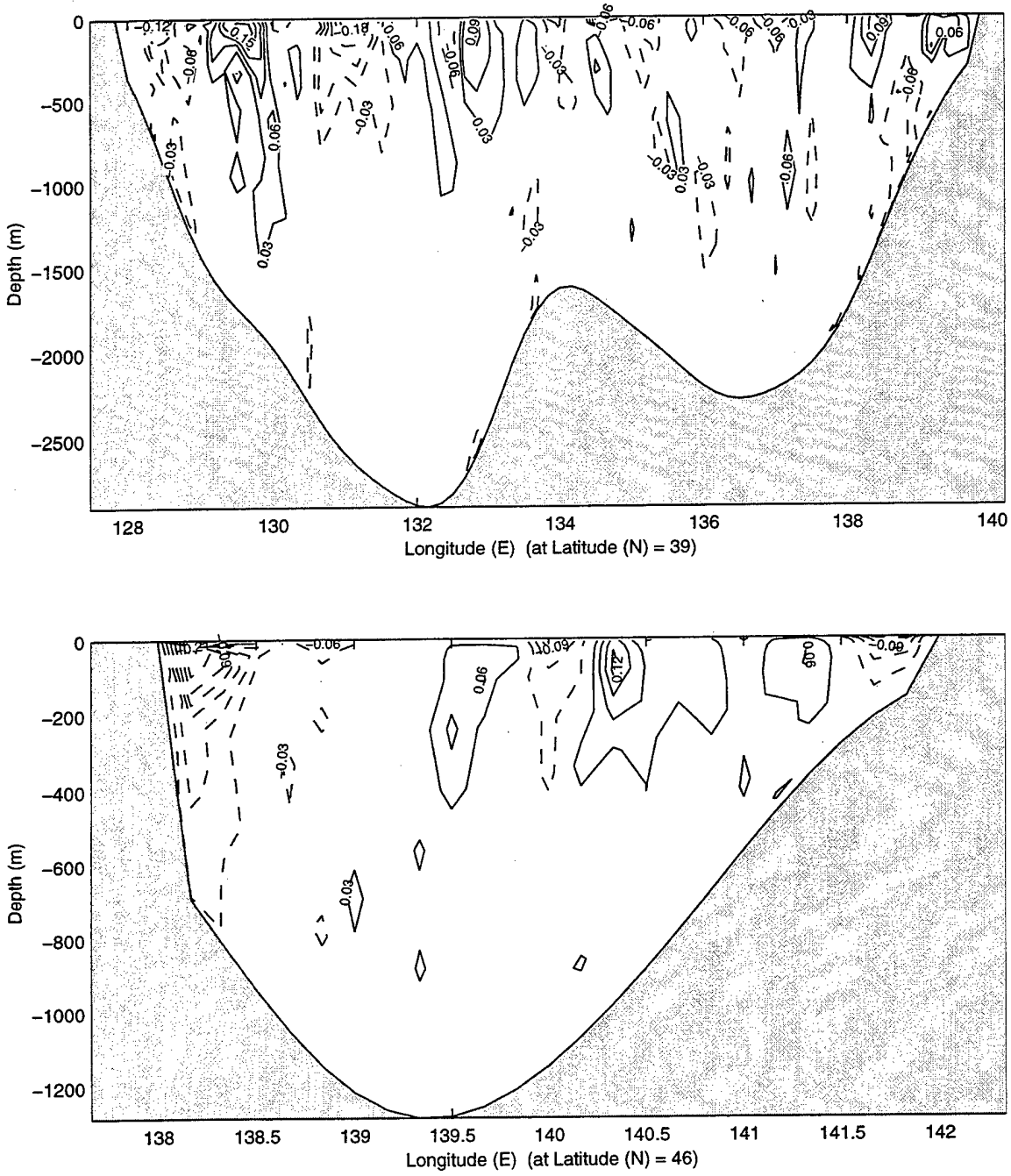

Fig. 17. V component of velocity (m/s) at latitudinal cross sections for January.

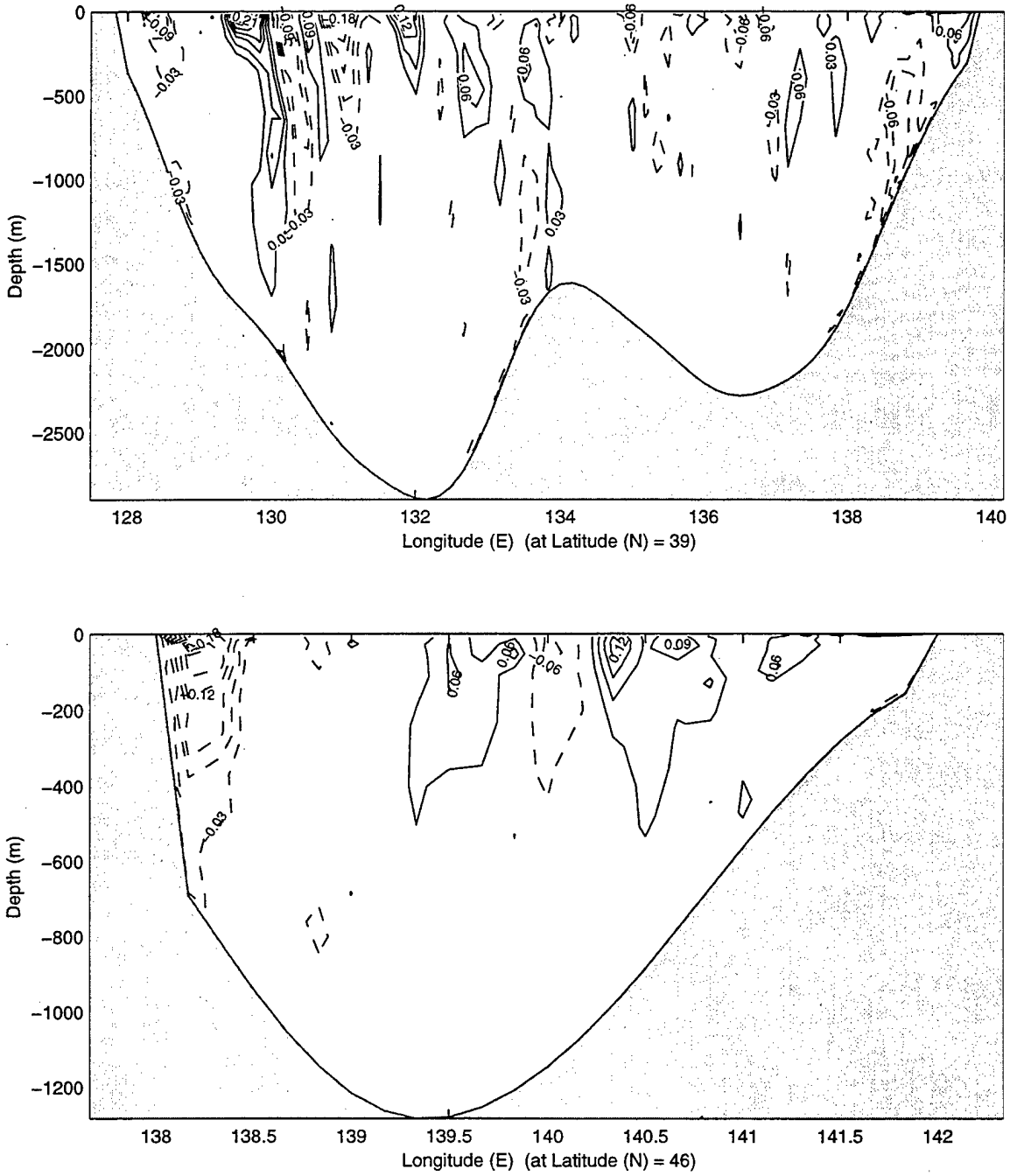

Fig. 18. V component of velocity (m/s) at latitudinal cross sections during April.

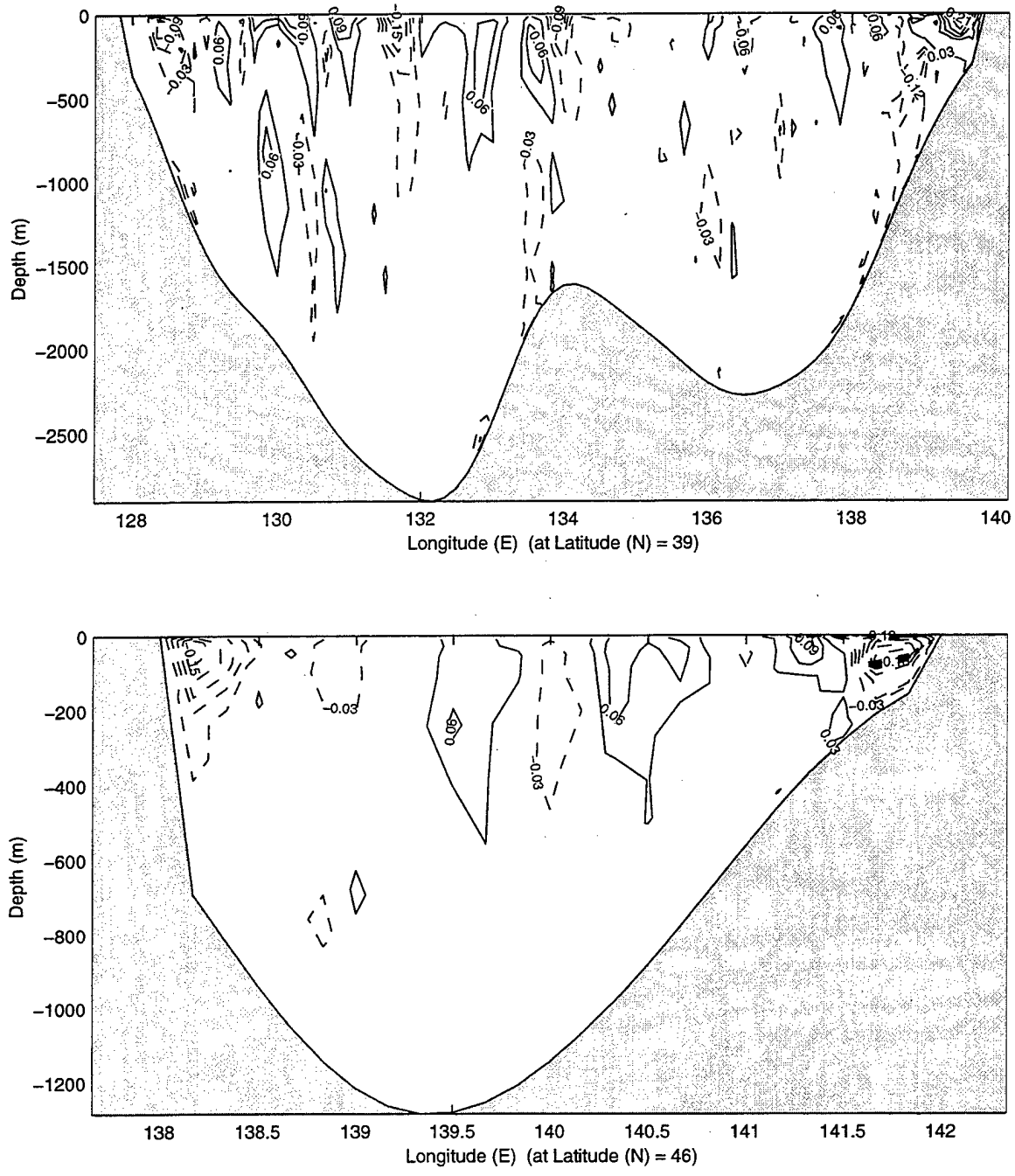

Fig. 19. V component of velocity (m/s) at latitudinal cross sections for July.

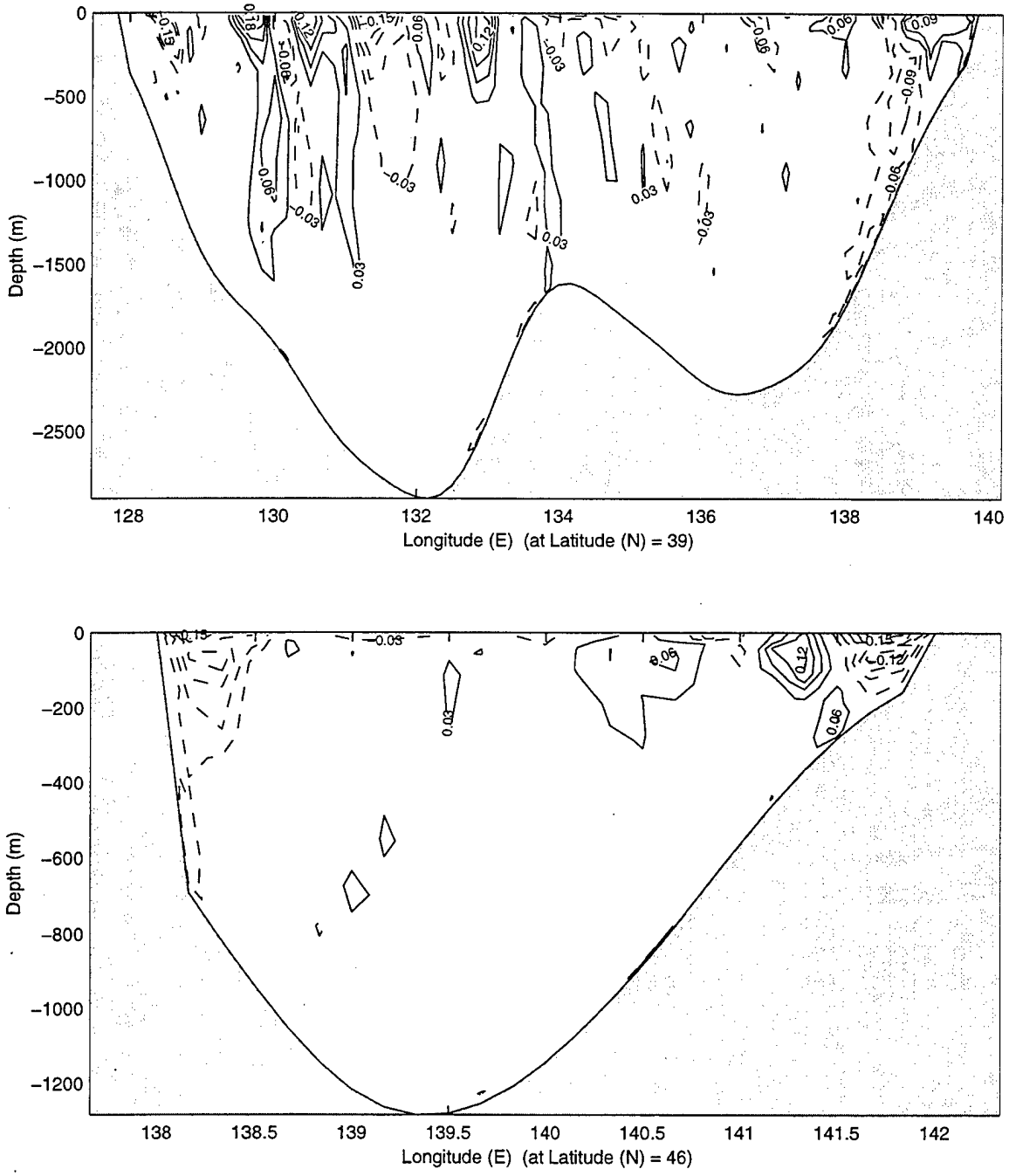

Fig. 20. V component of velocity (m/s) at latitudinal cross sections for October.

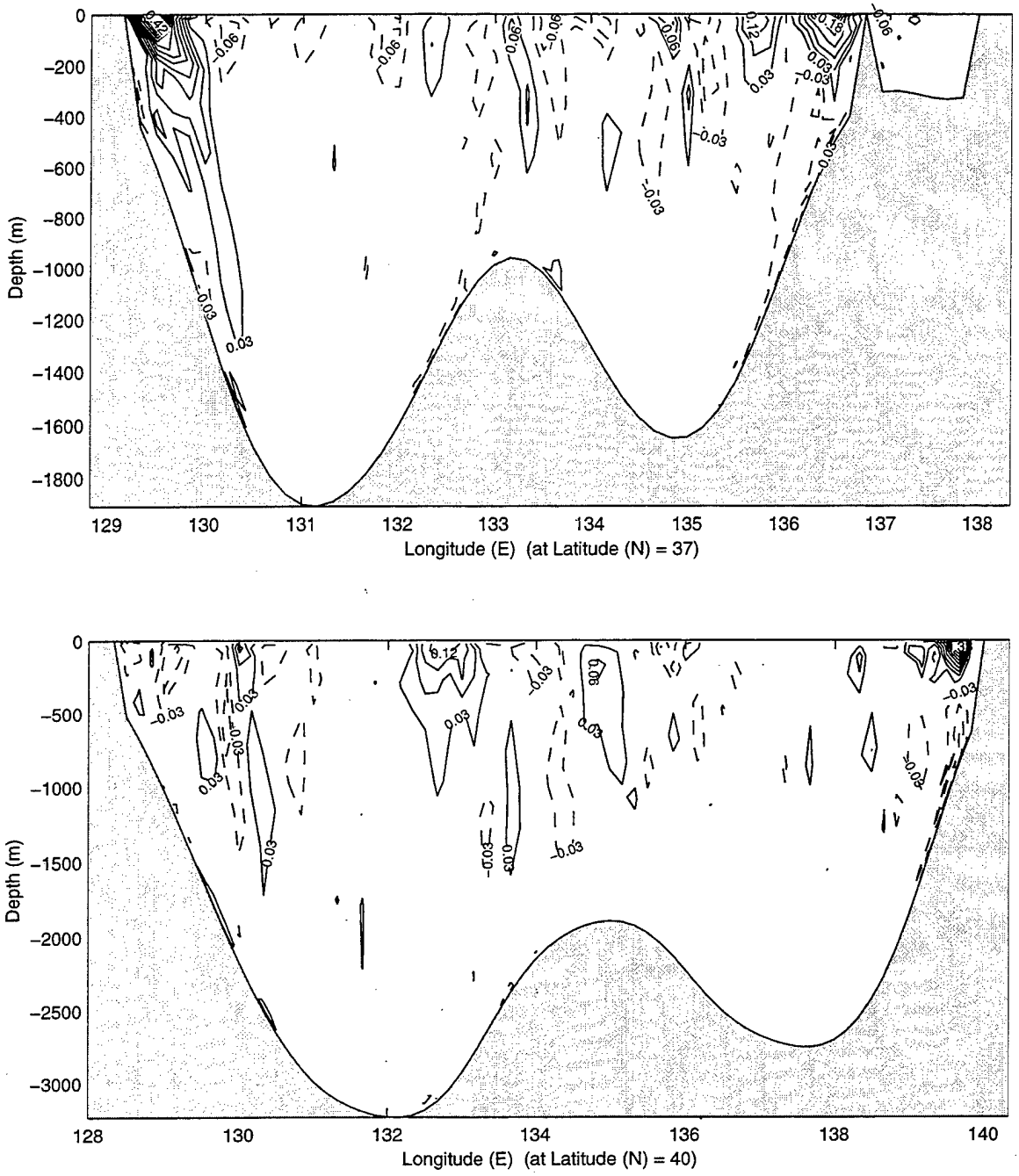

Fig. 21. V component of velocity (m/s) at latitudinal cross sections for July.

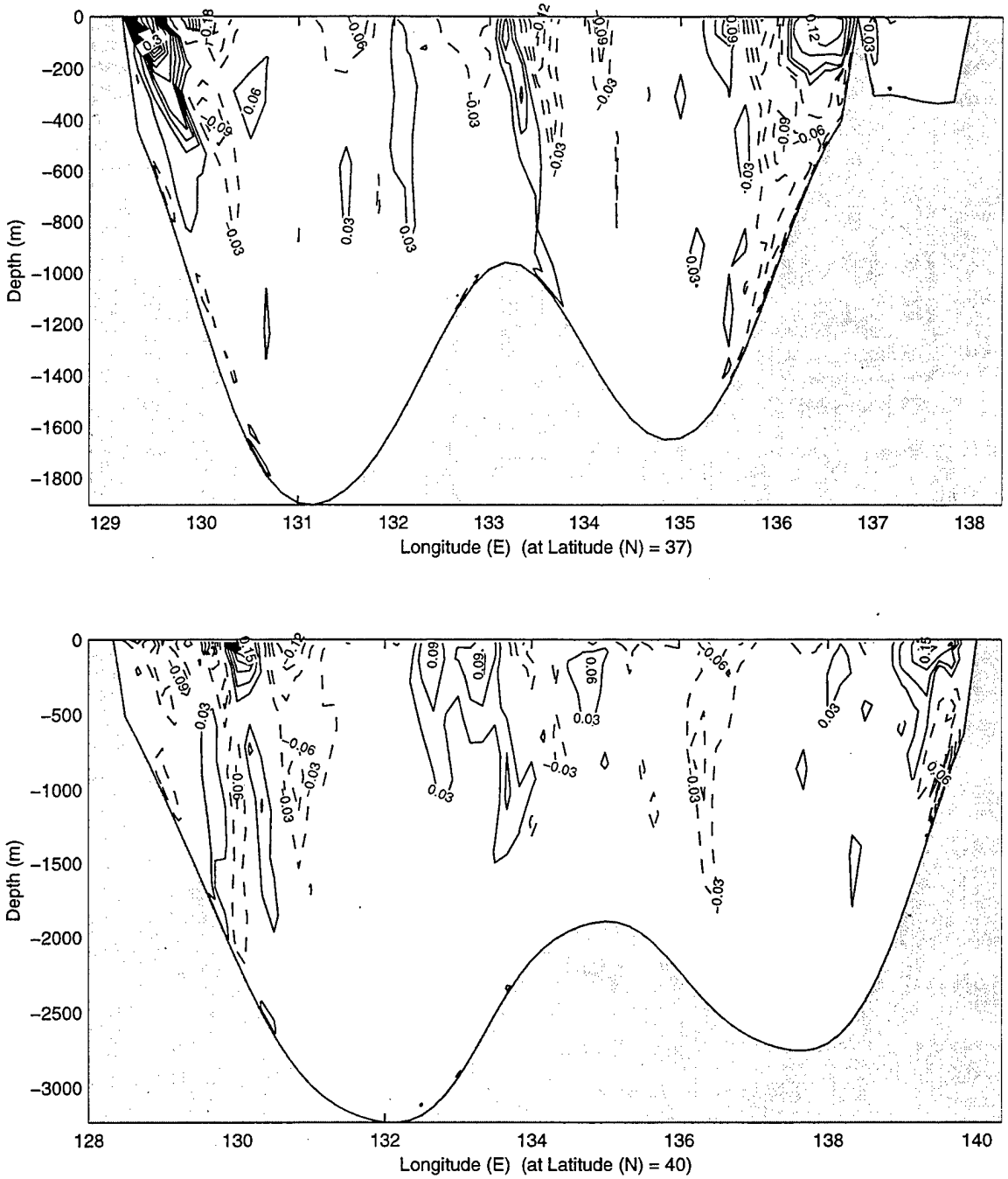

Fig. 22. V component of velocity (m/s) at latitudinal cross sections for January.

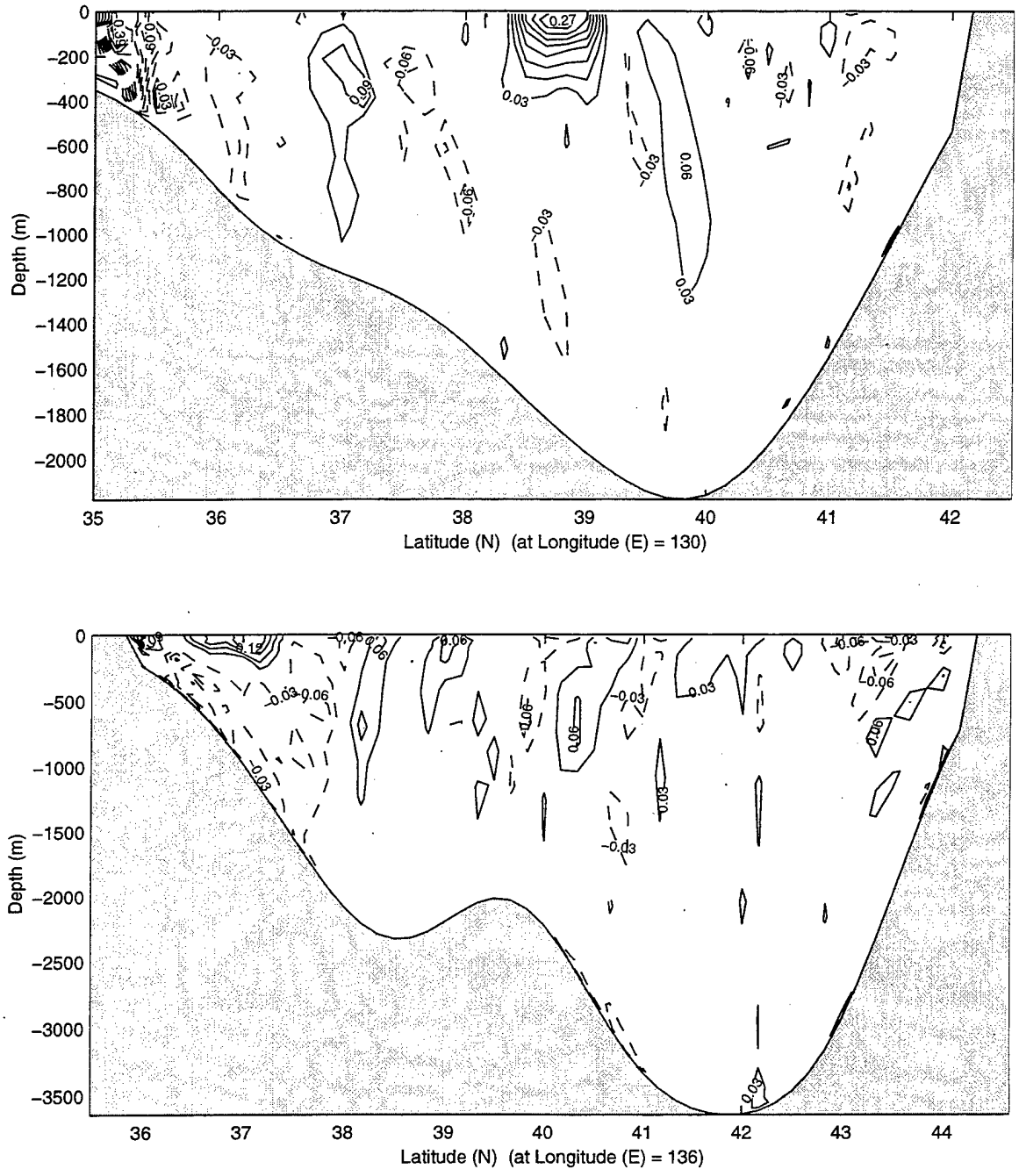

Fig. 23. U component of velocity (m/s) at longitudinal cross sections for October.

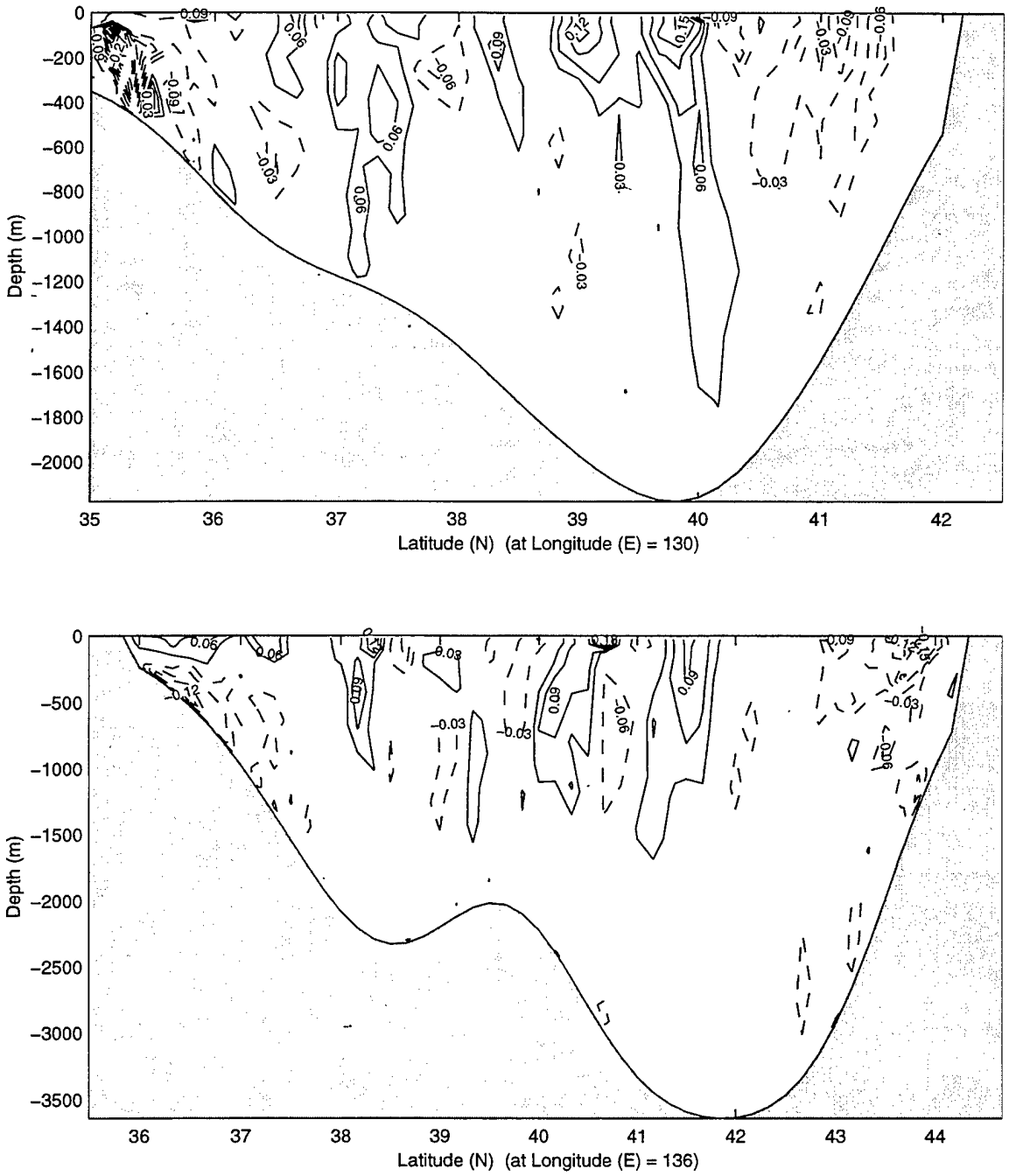

Fig. 24. U component of velocity (m/s) at longitudinal cross sections for January.

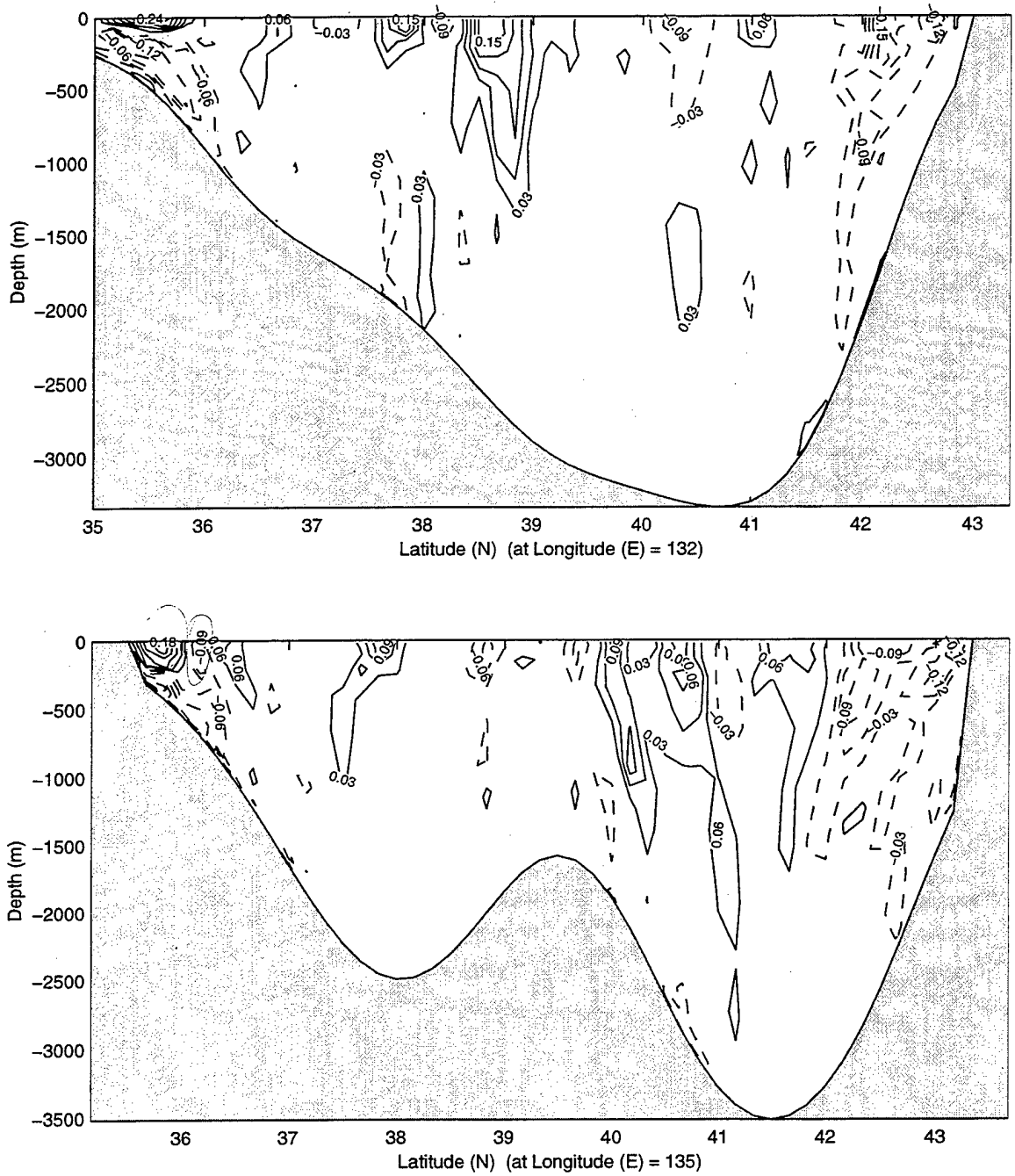

Fig. 25. U component of velocity (m/s) at longitudinal cross sections for January.

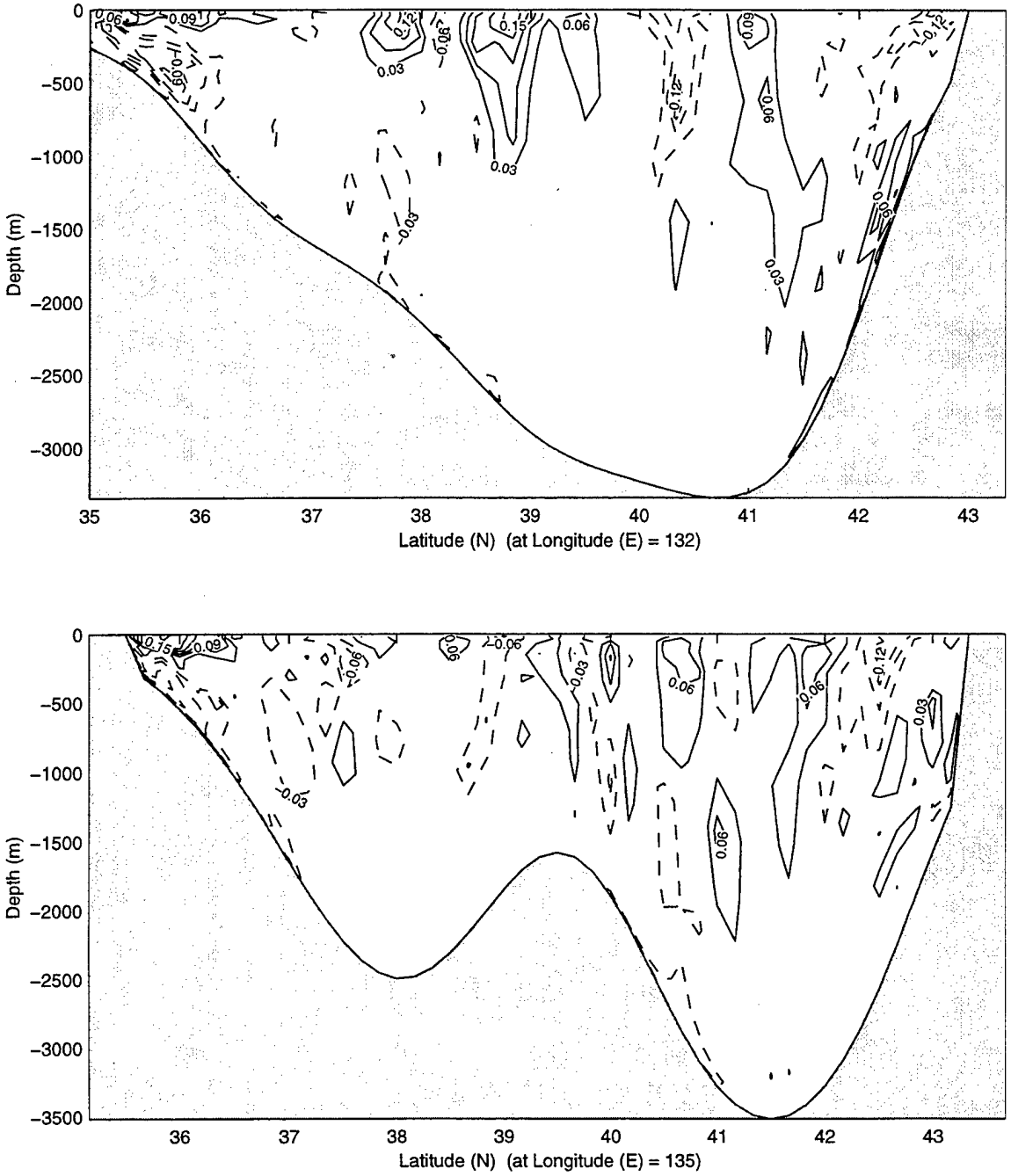

Fig. 26. U component of velocity (m/s) at longitudinal cross sections for October.

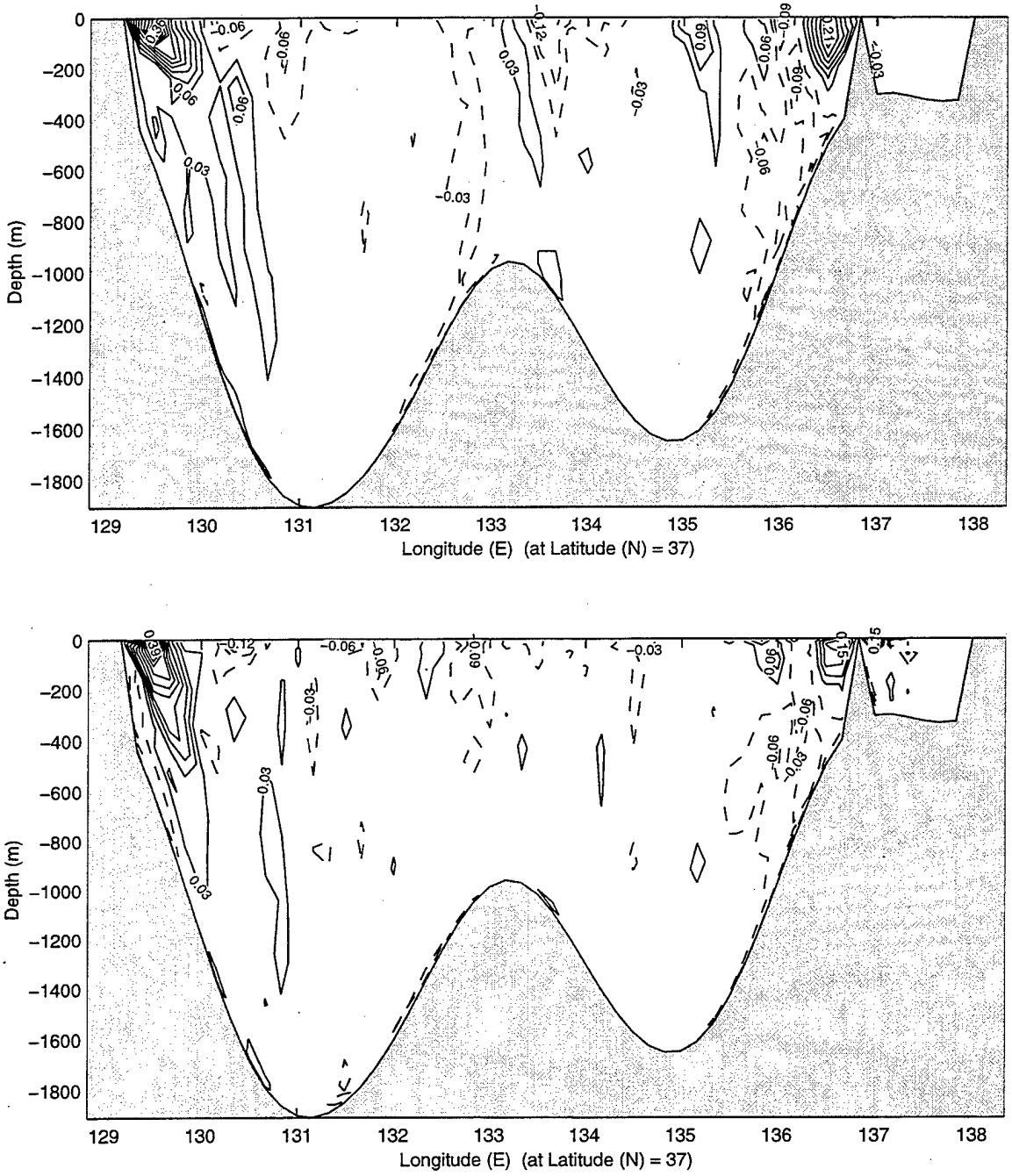

Fig. 27. V component of velocity (m/s) at latitudinal cross sections during (a) October and (b) April.

VI. DRIVING MECHANISMS

We analyzed the results of the four experiments to identify the driving mechanisms for the JES circulation.

A. EFFECTS OF NON-LINEARITY (RUN 1 – RUN 2)

In the first sensitivity study, the nonlinear advection terms were removed from the dynamic equations. Otherwise, the same parameters as the control run were used. The figures and analysis were performed after computing the difference between control and non non-linear terms runs. The differential surface vector velocities (Fig. 28) does not show evident general circulation patterns except couple mesoscale eddies, and especially the UB eddy, which indicates that the non-linearity does not change the general circulation pattern except for the UB anticyclonic eddy. However, our computation shows that the non-linearity causes a noticeable change in the volume transport (Fig. 29).

Fig. 29 shows the plots of the difference in the volume transport streamfunction (Ψ) for the control run minus the linear run and represents nonlinear effects. The major feature of Ψ is the multi-eddy structure with a strong cyclonic eddy with a minimum value of -6 Sv near the NKCC and EKWC confluence (131-133 E, 40-42 N). This indicates that the non-linear effect is responsible for the eddy generation. Besides, in the spring (Fig. 29b) there is a cyclonic gyre with a minimum value of –3 Sv in the JB, indicating that the non-linear effect might contribute nearly 60% to the JB cyclonic gyre.

B. EFFECTS OF WIND (RUN 1 – RUN 3)

The difference between Run 1 and Run 3 shows the monsoon wind effects. The winter wind effect on the surface circulation (Fig. 30a) and the volume transport (Fig.

31a) is in contrast to the summer wind forcing (Figs. 30c and 31c). The winter wind forcing causes a strong basin-wide JES cyclonic gyre (Fig. 31a) with 8 Sv recirculation and the summer wind forcing drives a weak nearly basin-wide JES anticyclonic gyre (Fig. 31c). Similar patterns and values are found between Ψ (Fig. 31) and Ψ for the control run (Fig. 16) in the northern JES for all the seasons. This indicates that the wind forcing is the most important factor (80%) for the generation of the JB cyclonic gyre. Different patterns and values are found between Ψ (Fig. 31) and Ψ_c (control run) (Fig. 16) in the southern JES in the winter: negative values for Ψ and positive values for Ψ_c. This indicates that the wind forcing in the winter weakens the southern JES circulation.

Compared to the surface velocity vector map for the control run (Fig. 15), the surface differential current vectors $\Delta\mathbf{V}$ (Fig. 30) clearly show the wind effects on the JES circulation: (a) driving the LC in the winter, (b) damping the EKWC especially in the winter, (c) generating the UB eddy in all the seasons, and (d) generating eddies along the JCC. The wind has almost no effect on the occurrence of the JCC for all seasons.

The winter monsoon winds blow from the northwest to the southeast over the JES surface (Fig. 3) and drives the Ekman flow in the upper ocean to the right of the wind direction. Such a surface current moves southward at the western coast of the JES and strengthens the LC and weakens the EKWC. The LC strengthens in the winter by 30% (v-component 0.06 m/s southward) due to wind at 46°N (Fig. 32b). The summer monsoon winds blow from the south and southeast to the northwest with much smaller speeds. Thus, the summer wind effects on reducing LC and strengthening EKWC are quite weak.

The winds drive mesoscale eddies especially near UB and along the west coast of Honshu. The surface UB eddy, occurring on the differential velocity vector map (Fig. 30), has the similar swirl velocity (anticyclonic) with same order of magnitudes (maximum value of 0.7 m/s) as the control run (Fig. 14). This means that the wind effect is in fact a key factor for generating the UB anticyclonic eddy. Furthermore, there is no evident current along the west coast of Honshu on the $\Delta \mathbf{V}$ map (Fig. 30), indicating that wind forcing is not a major factor for maintaining JCC.

C. EFFECTS OF LATERAL BOUNDARY TRANSPORT (RUN 1 – RUN 4)

The third sensitivity study used the control run equations and forcing but closed all open lateral boundaries, preventing the transport of mass, heat or salinity through the Tsushima, Tsugaru, Soya, and Tatar Straits. With inflow or outflow, the JES vertically integrated circulation pattern is more pronounced in the summer than in the winter. This is because Ψ (control – no transport) pattern (Fig. 33) is quite similar to Ψ_c (control run) (Fig. 16) in the summer than in the winter. Increased circulation in the summer by the lateral transport generally leads to greater horizontal and vertical variabilities of the current structure. In the winter, Ψ has positive values (2 Sv), and Ψ_c has negative values in JB. This suggests that the lateral transport reduces the JB cyclonic gyre by 2 Sv in the winter.

Compared to the surface velocity vector map for the control run (Fig. 15), the surface differential current vectors $\Delta \mathbf{V}$ (Fig. 34) clearly show the lateral transport effects on the JES circulation: (a) driving the UB eddy in all the seasons, (b) generating EKWC, and (c) generating JCC and eddies along the JCC.

An eddy over the Ulleung Basin (38°N 130°E) is well depicted in the summer surface $\Delta\mathbf{V}$ field (Fig. 34c). The calculated swirl velocity is 0.25 m/s at 39°N 130°E (Figs. 35a and 36a); similar magnitude to what was observed in the non-linear effect. However, the depth ranges from 300-600 m, which are shallower than the non-linear case.

Along the East Korean Coast in the winter, Δv has a value of 0.15 m/s at 37°N (Fig. 37a), 50% of the v-component in the control run. Finally, at 40°N 130°E the calculated $|\Delta\mathbf{V}|$ is 0.21 m/s to the northeast direction (Figs. 37b and 38a), reaching a depth of 1400m. This corresponds to 100% of $|\mathbf{V}|$ in the control run (Figs. 22b and 24A). This suggests that in the winter the lateral transport contributes 50% (100%) to the EKWC in the southern (northern) Korean Coast. In the summer, Δv has a velocity of 0.09 m/s at 37°N (Fig. 39a), or 21% of the v-component in the control run.

The lateral transport has very weak effects on the occurrence of the LC current for all seasons. The LC strength in the winter is 30% due to the lateral transport at 46°N (Fig. 40b).

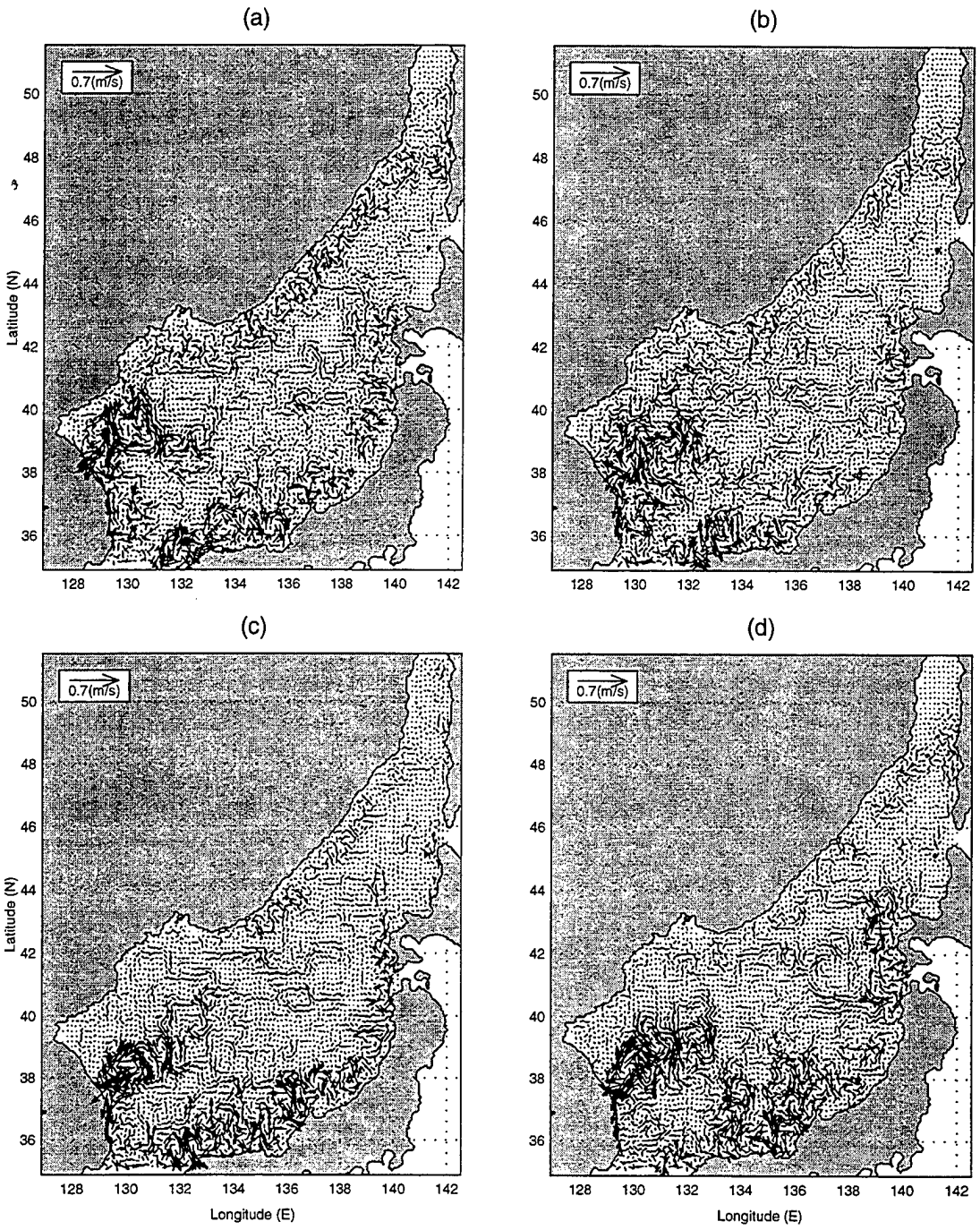

Fig. 28. Surface circulation from non-linear effects for (a) January, (b) April, (c) July and (d) October.

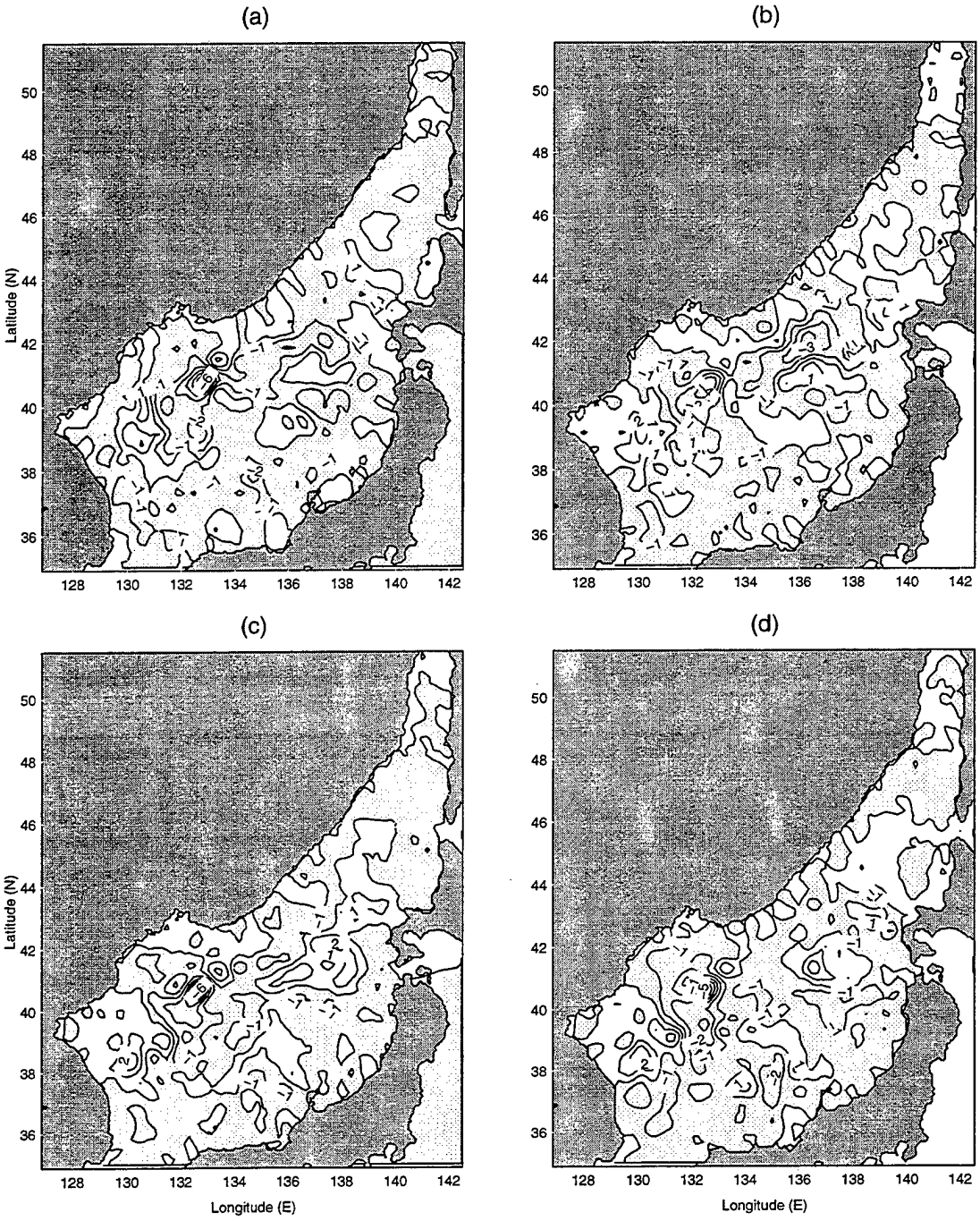

Fig. 29. Volume transport from non-linear effects for (a) January, (b) April, (c) July and (d) October.

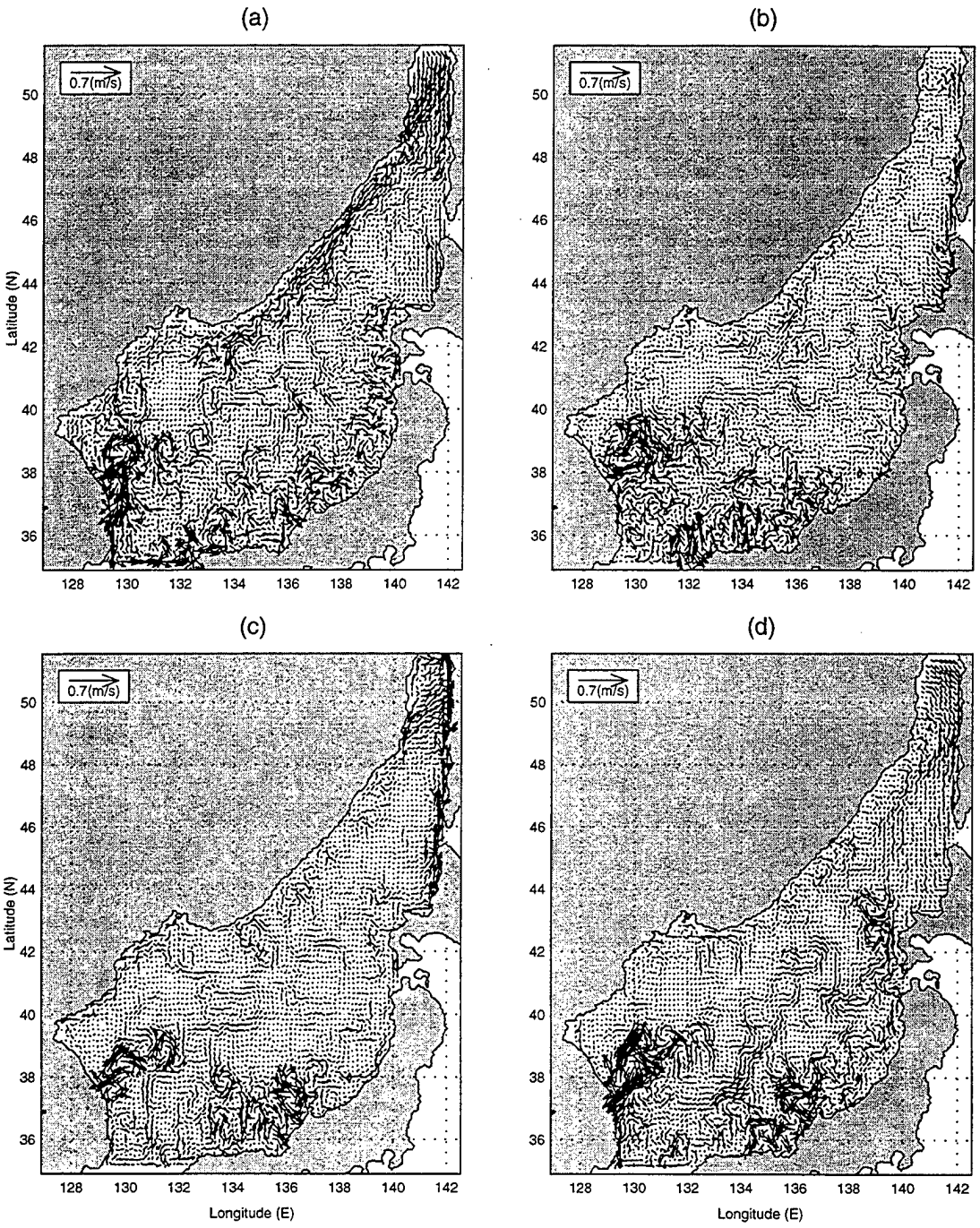

Fig. 30. Surface circulation from no wind effects for (a) January, (b) April, (c) July and (d) October.

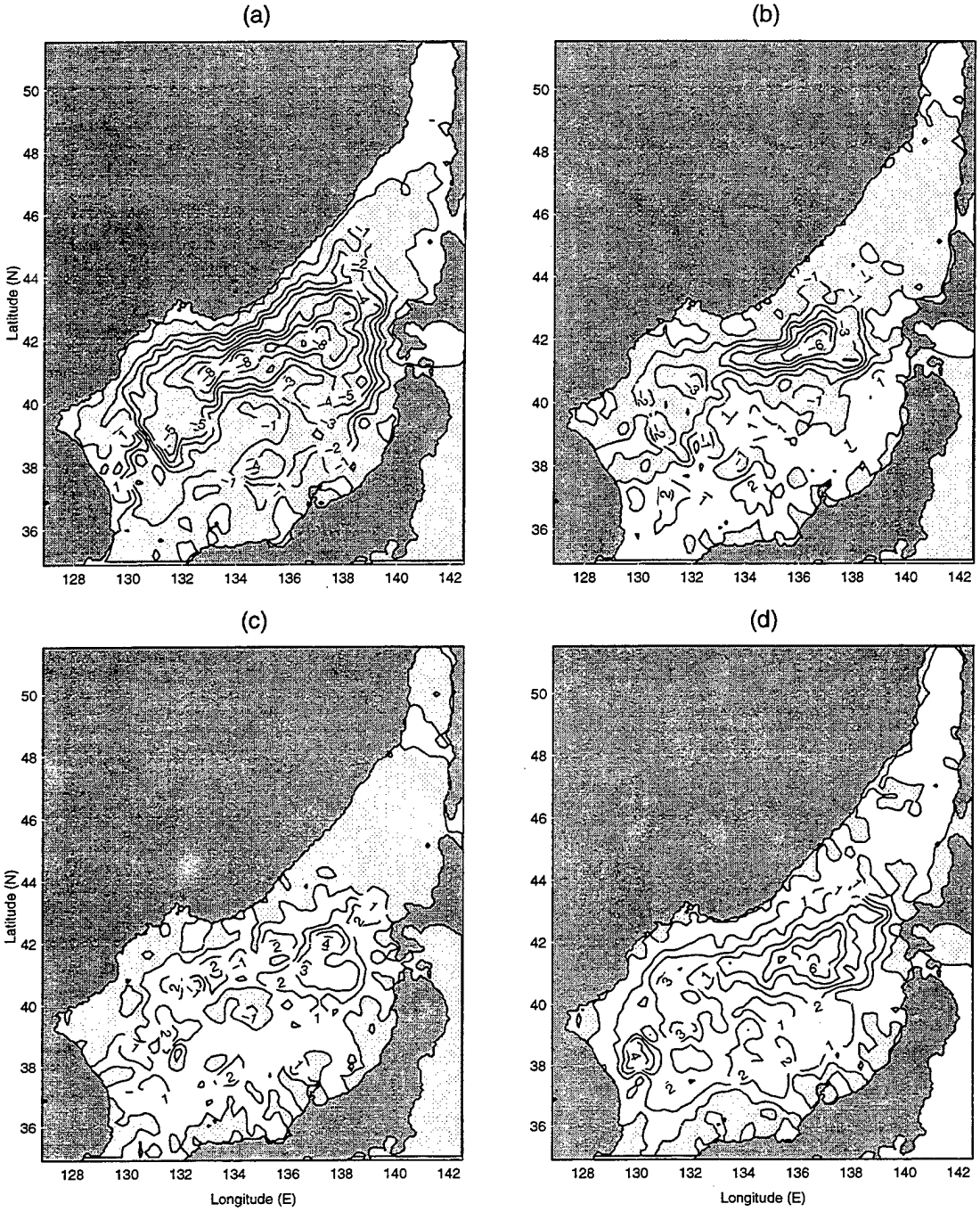

Fig. 31. Volume transport from no wind effects for (a) January, (b) April, (c) July and (d) October.

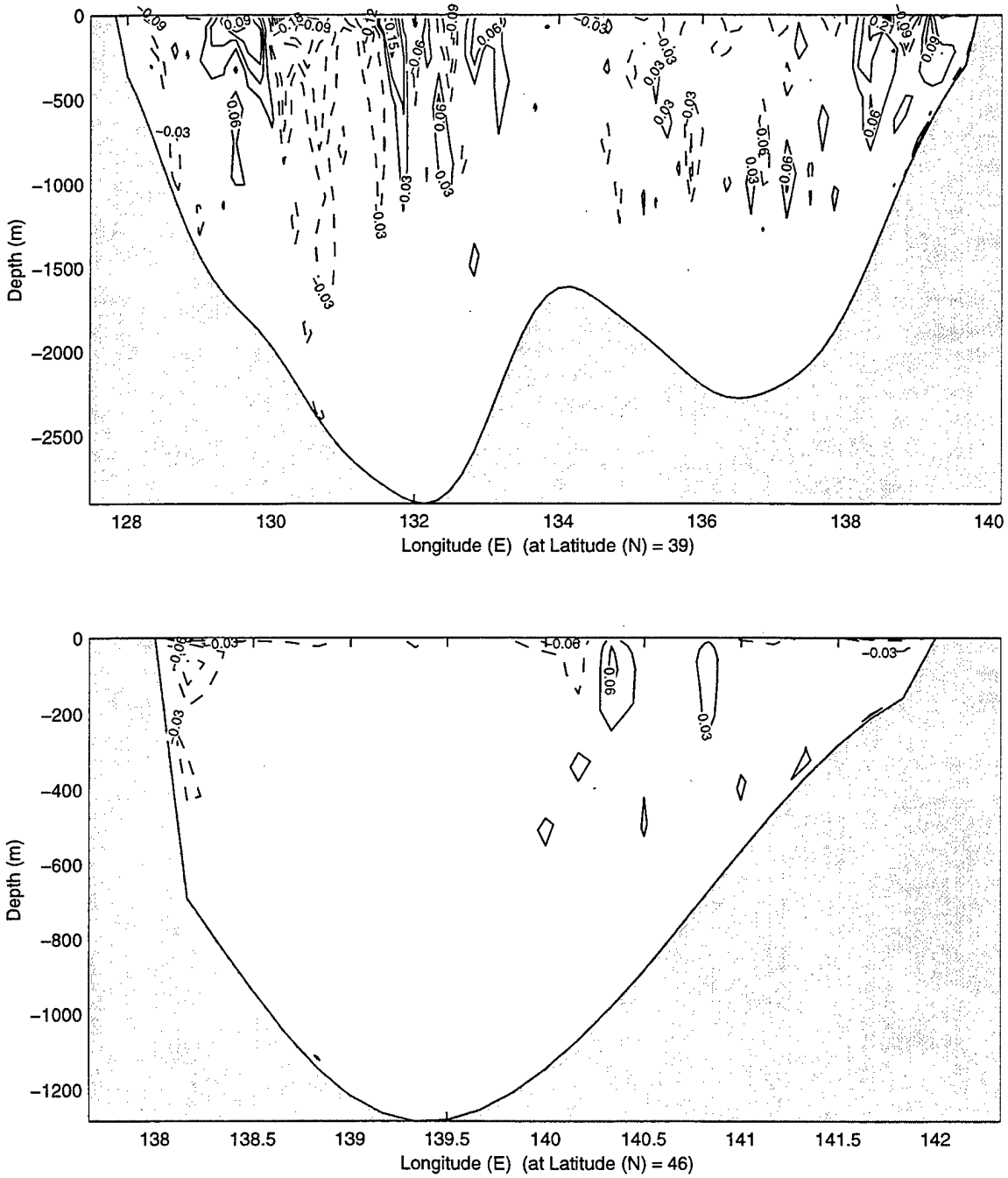

Fig. 32. V component of velocity (m/s) at latitudinal cross sections from no wind effects for January.

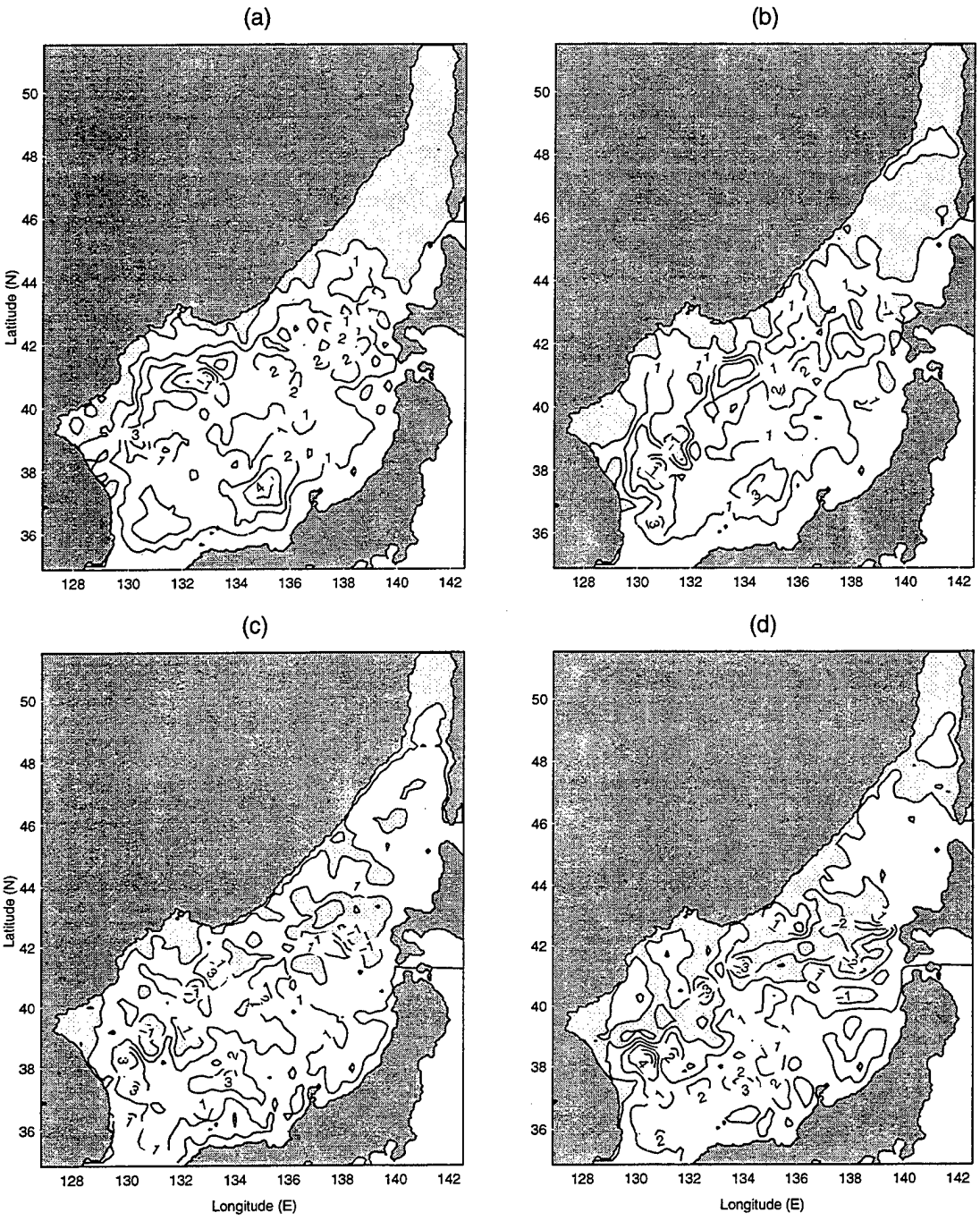

Fig. 33 Volume transport from no lateral transport effects for (a) January, (b) April, (c) July and (d) October.

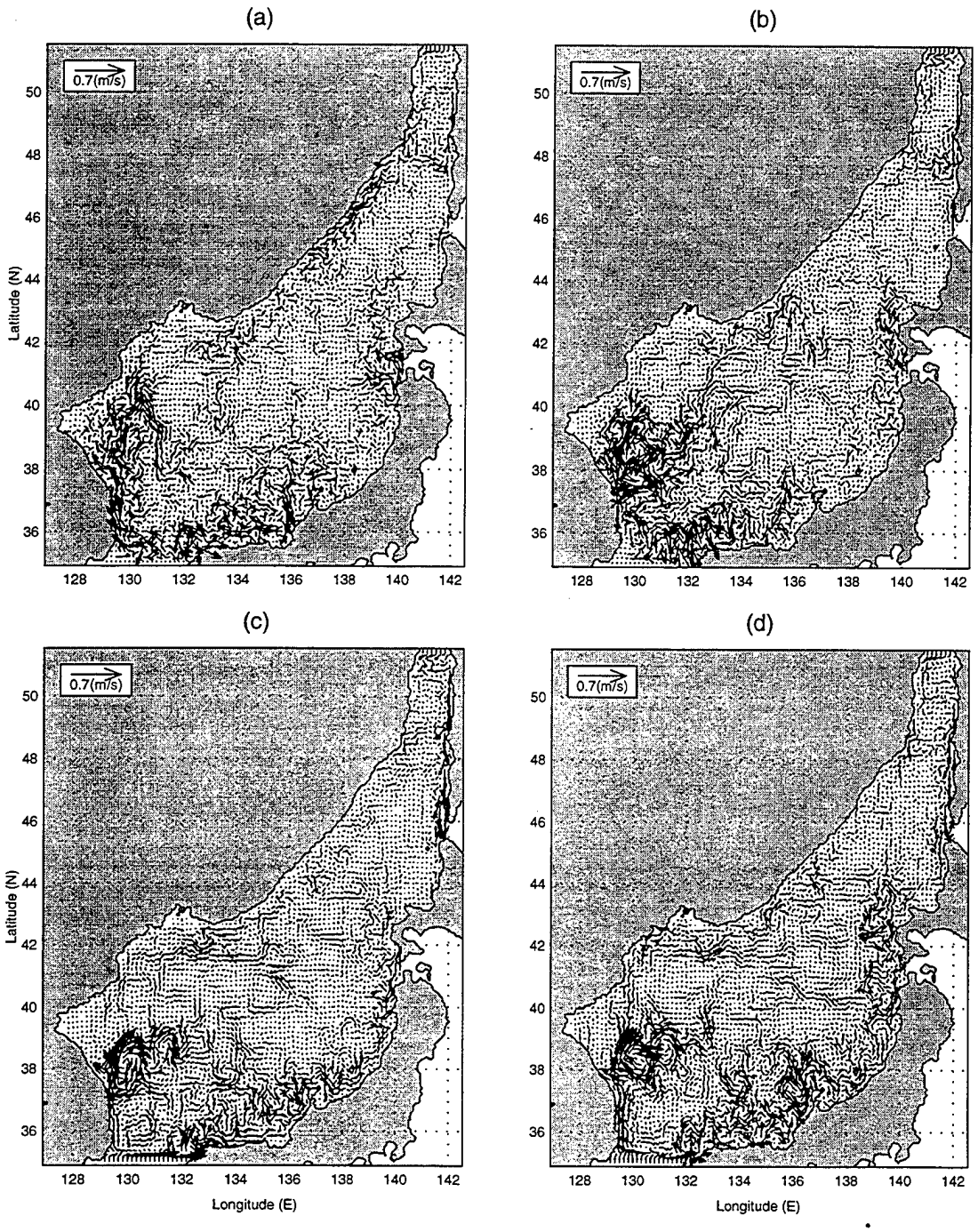

Fig. 34. Surface circulation from no lateral transport effects for (a) January, (b) April, (c) July and (d) October.

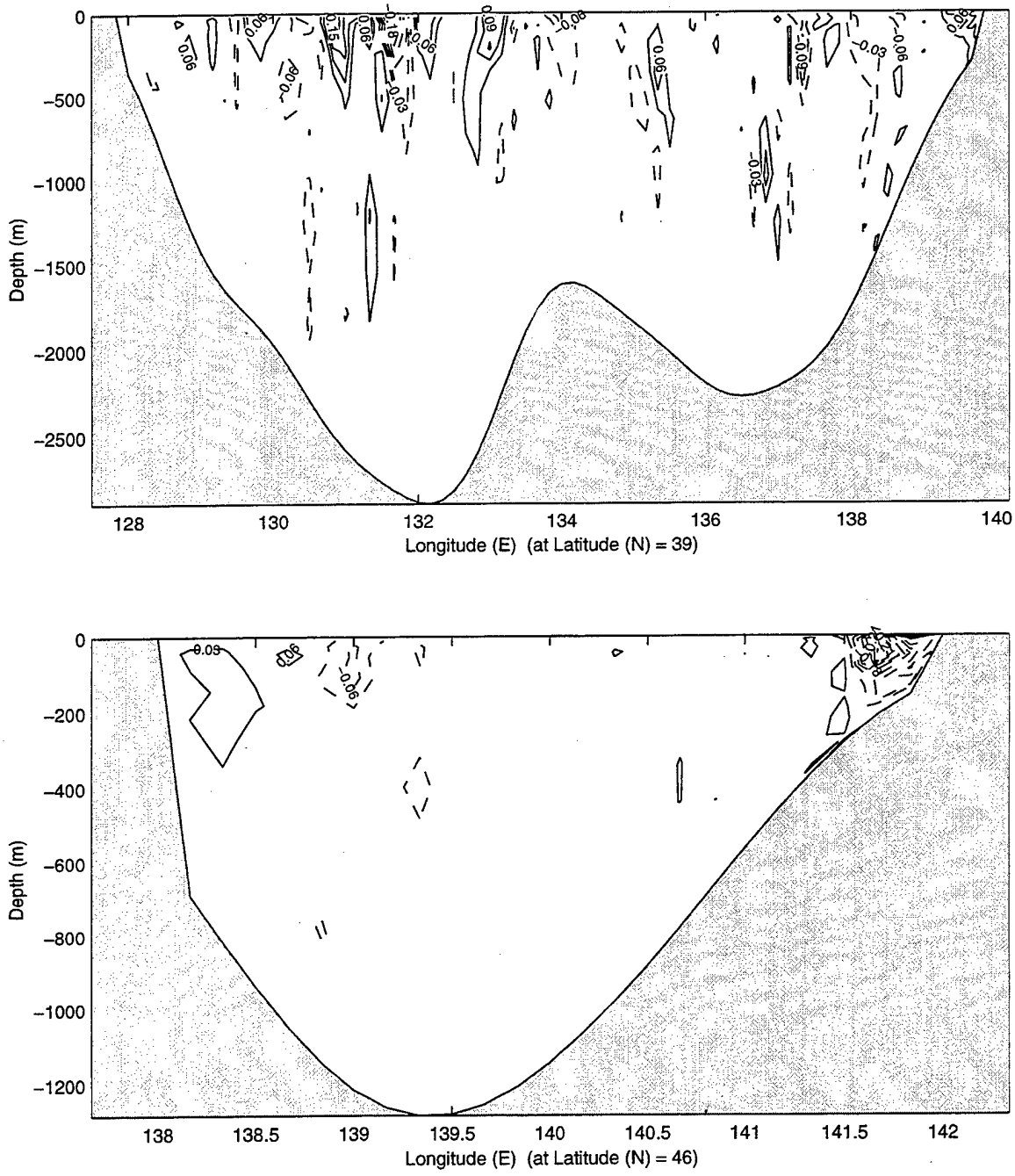

Fig. 35. V component of velocity (m/s) at latitudinal cross sections from no lateral transport effects for July.

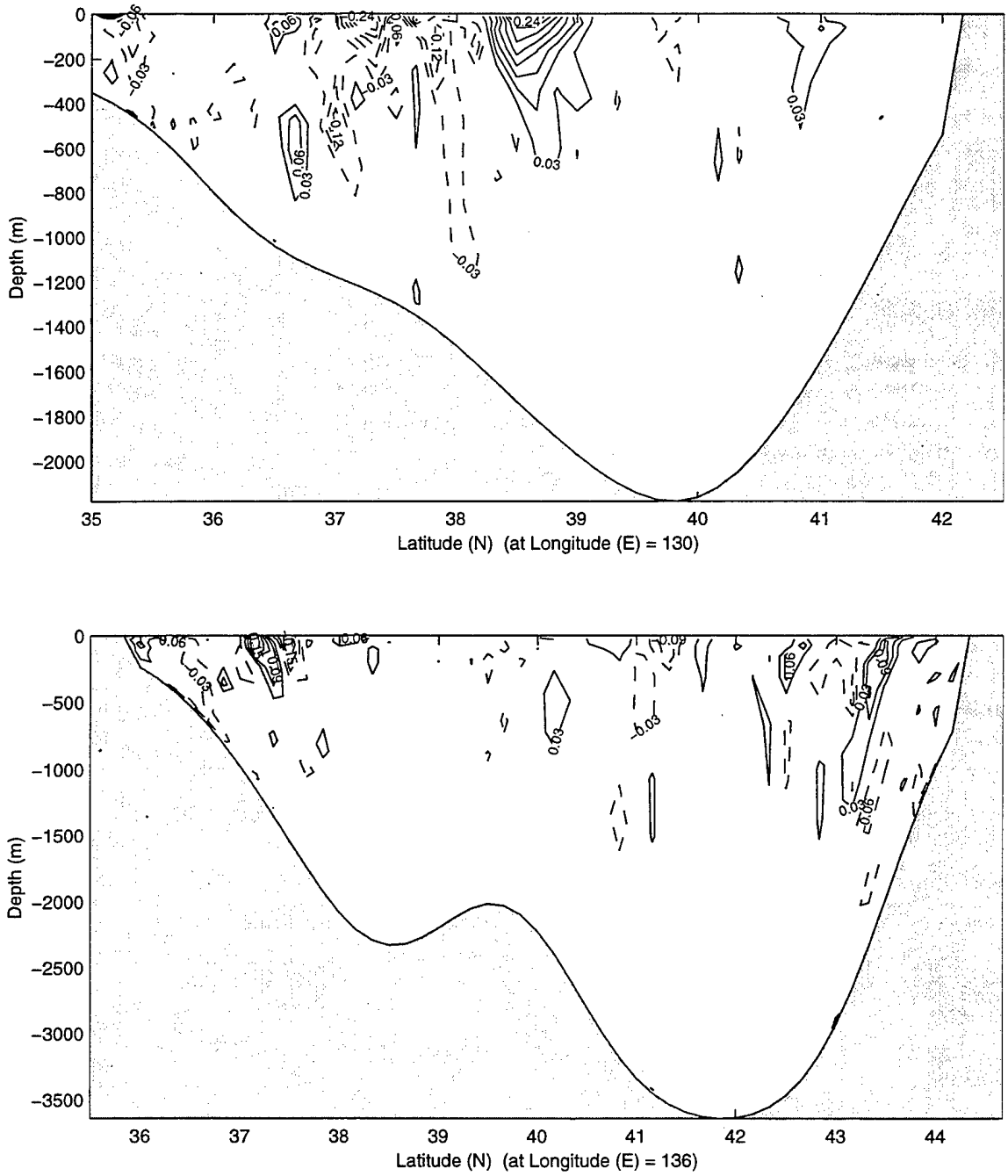

Fig. 36. U component of velocity (m/s) at longitudinal cross sections from no lateral transport effects for July

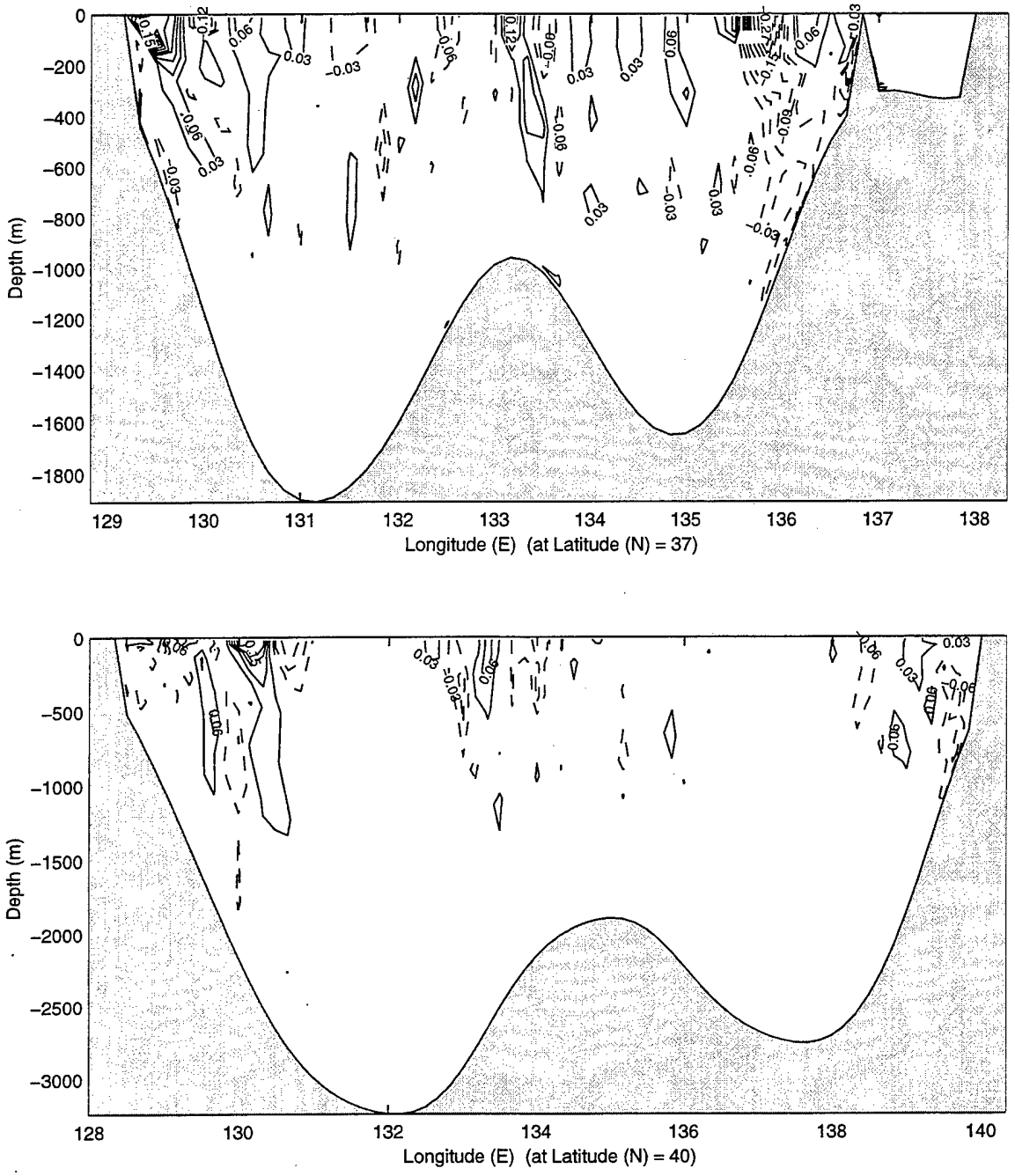

Fig. 37. V component of velocity (m/s) at latitudinal cross sections from no lateral transport effects for January.

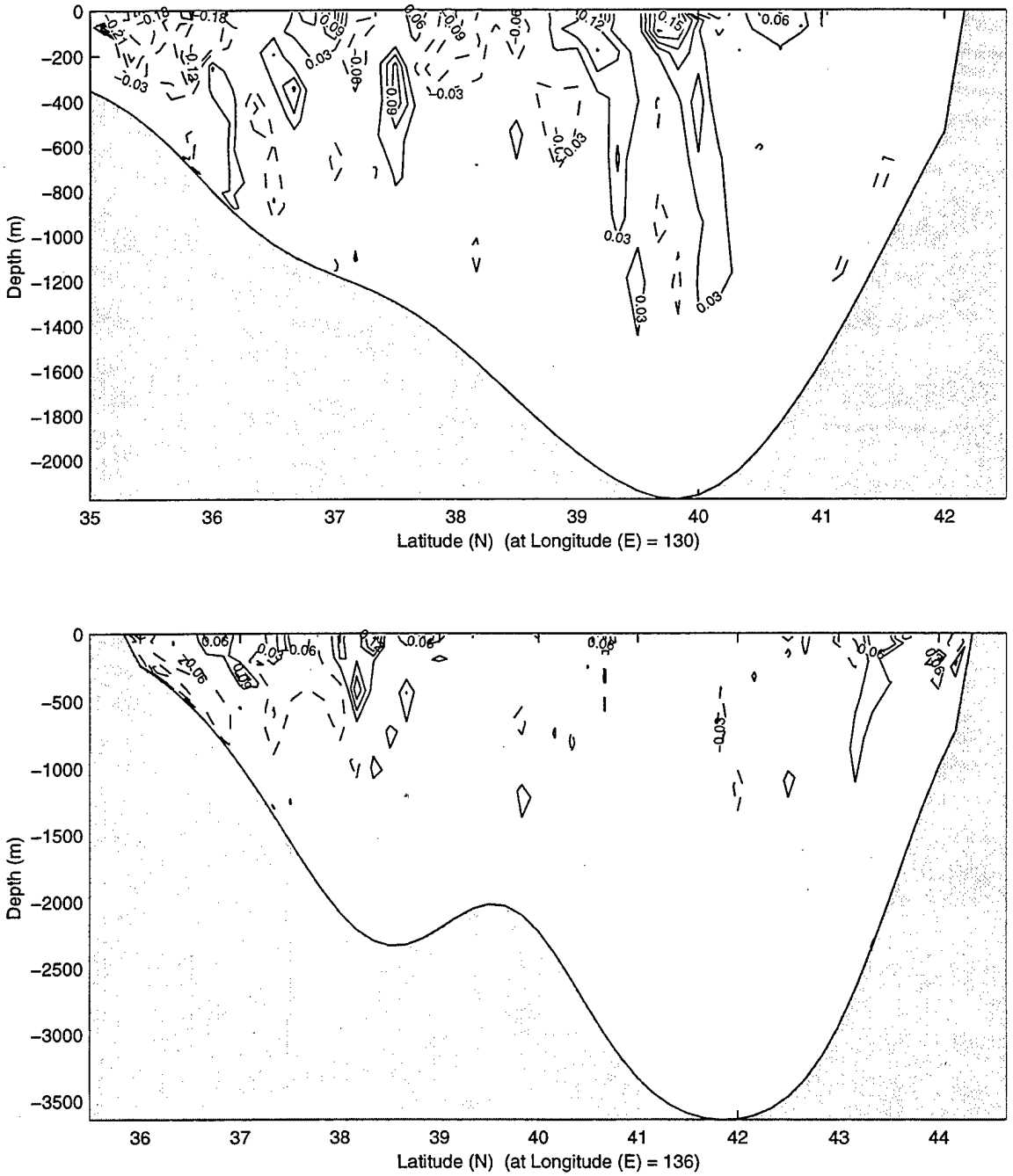

Fig. 38. U component of velocity (m/s) at longitudinal cross sections from no lateral transport effects for January.

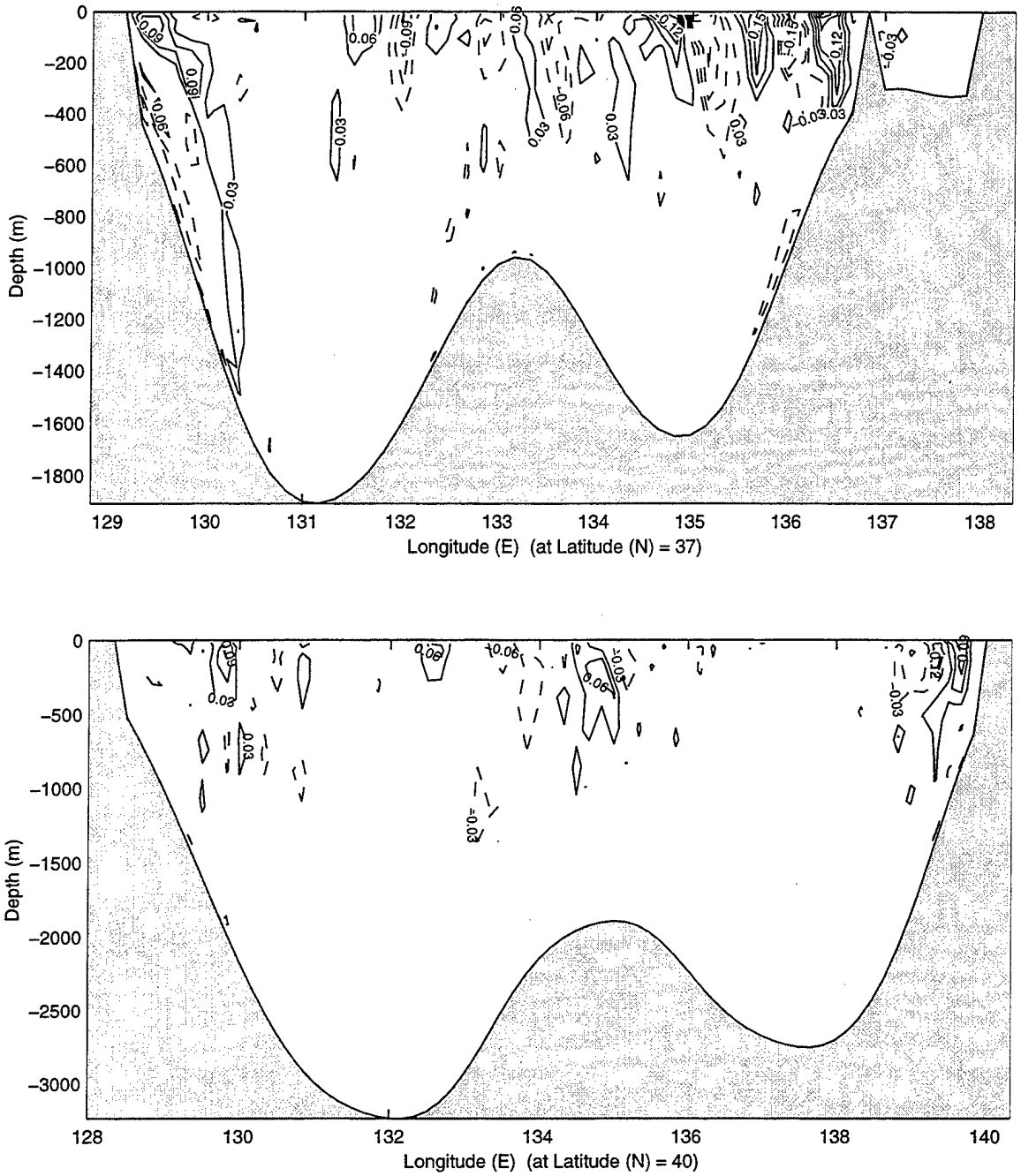

Fig. 39. V component of velocity (m/s) at latitudinal cross sections from no lateral transport effects for July.

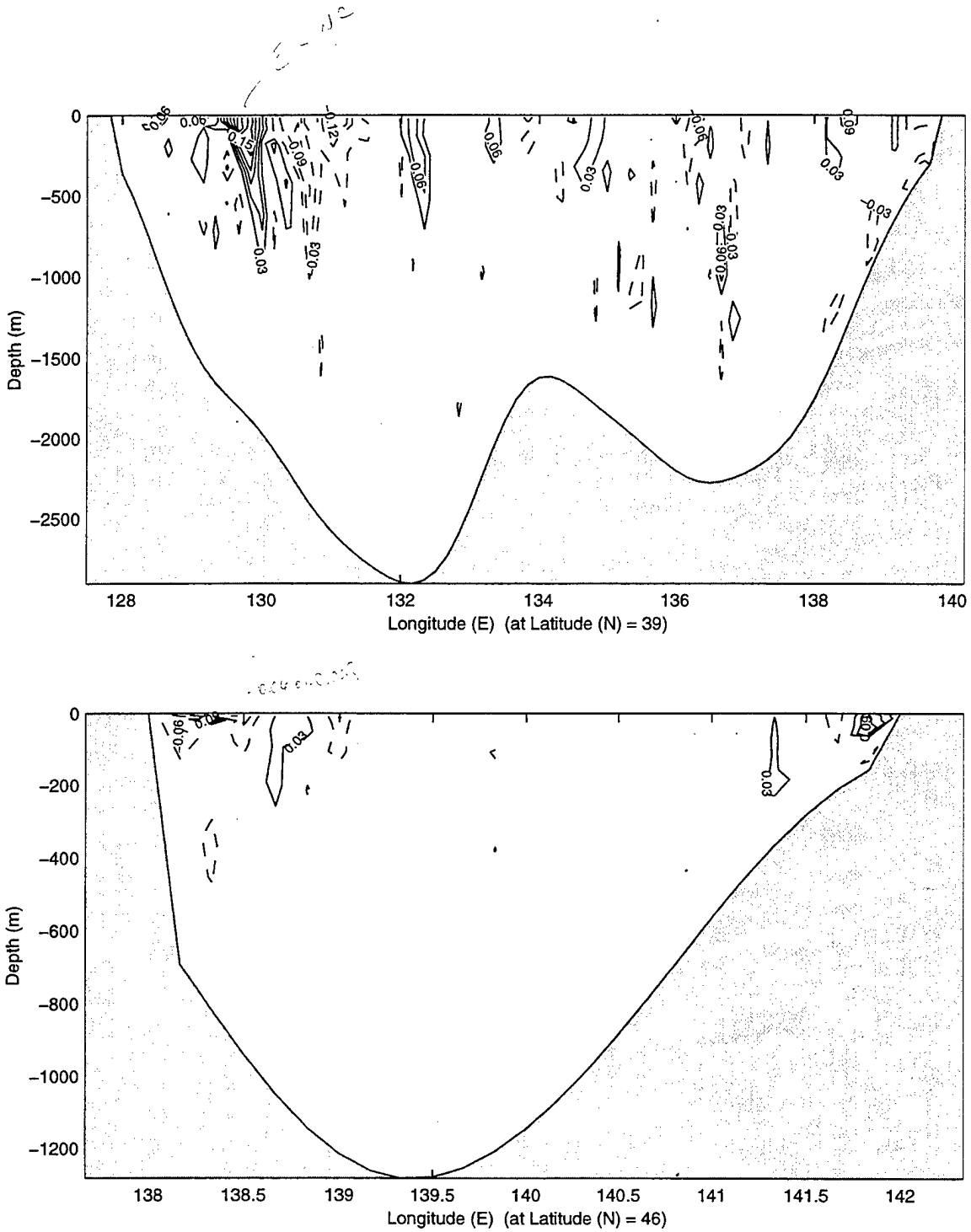

Fig. 40. V component of velocity (m/s) at latitudinal cross sections from no lateral transport effects for January.

THIS PAGE INTENTIONALLY LEFT BLANK

VII. CONCLUSIONS

(1) The JES circulation and thermohaline structure was simulated in this study by the POM model under the climatological forcing. The northern JES is occupied by a cyclonic gyre (called the JB gyre) and the southern JES is characterized as a multi-eddy structure. The volume transport streamfunction has a double-gyre structure with negative values (cyclonic) in the northern JES and positive values (anticyclonic) in the southern JES. It has an evident seasonal variation with the appearance of the cyclonic gyre in the northern JES (i.e., the JB) in the winter and spring and disappears in the summer and fall.

(2) A large-scale cyclonic recirculation gyre over the JB is simulated with a strong seasonal variation. The JB cyclonic gyre is the strongest and recirculates 8 Sv in the winter. It weakens and retreats northward in the spring and summer. In the fall, the cyclonic JB gyre disappears and weak anticyclonic eddies appear.

(3) The POM model simulates the basic currents in the JES such as the LC, EKWC, NKCC, and JCC. The LC has a maximum southward component (0.21 m/s) and occurs near the surface in the winter with a width of 100 km and a depth of 800 m. The core of the LC is close to the coast and near the surface. In the spring, its strength weakens to 0.18 m/s, but the width and depth remain almost unchanged. It further weakens to a minimum of 0.15 m/s in the summer and fall, and shrinks in size to a width of 60 km and depth of 400 m. The EKWC, the western branch of the TC north of the Tsushima/Korea Strait, acts as a western boundary current varying from 0.42 m/s (summer) to 0.30 m/s (winter). The width of the EKWC is around 60 km all year round. However, the depth is around 1,400 m in the summer and 800 m in the winter. The

(northward) overshot EKWC leaves the Korean coast and moves northward. It converges with the southward flowing NKCC, at 40°N, 130°E, and forms a current meandering toward east along the Polar Front, defined as the Polar Front Current (PFC). The resultant velocity of the PFC is 0.32 m/s and northeastward, in the fall, and 0.21 m/s in the winter.

The JCC, the eastern branch of the TC north of the Tsushima/Korea Strait at 132°E, has a maximum eastward component of 0.24 m/s in the winter. A counter current beneath it is simulated with the westward component of 0.12 m/s. In the summer, the counter current keeps almost unchanged, but the JCC falls down to 0.09 m/s. This is consistent with the observational study reported by Seung and Yoon (1995). The effect of coastal geometry, such as the Noto Peninsula on the JCC, is also simulated.

(4) The UB warm-core anticyclonic eddy is also simulated. The western branch of the warm TC (i.e., EKWC) moves northward along the southern part of the Korean coast and separates from the coast after approaching the East Korean Bay (EKB). It keeps its northward motion until meeting the NKCC near 40°N, meanders southeastward, and forms a warm-core anticyclonic eddy. The simulated anticyclonic UB eddy is strongest in the summer. The center is located at 38.5°N 130°E. The size of the eddy is around 150 km. The tangential velocity is around 0.4 m/s.

(5) The POM simulates the formation of the JES Polar Front and its seasonal variation. The simulated thermal field shows a strong north-south thermal asymmetry across the Polar Front. At a depth deeper than 500 m, the temperature is uniformly cold (1-2°C). In the winter, the thermocline appears in the southern JES, and disappears north of 41°N. The strength decreases with latitude from 7°C/100m near the Japan coast to less

than 1°C/100m at 40°N. In the summer, a strong seasonal thermocline, caused by strong surface heating, is simulated in the shallow depths overlying the permanent thermocline. The seasonal thermocline is sustained from summer to fall.

(6) The POM simulates the salinity field reasonably well with the surface featured by (a) higher salinity in the winter than in the summer; (b) stronger seasonal variability in the south than in the north of the Polar Front; and (c) two salinity activity centers located at the Tatar Strait and the Tsushima Strait. The model also simulates a strong north-south salinity asymmetry across the Polar Front with the salty tongue (34.1 psu) appearance only in the south of the Polar Front. The shallow and strong halocline associated with strong thermocline makes the sub-surface water mass north of the Polar Front hydrostatically stable. The mid-level salty tongue associated with weak and wide thermocline makes the water mass hydrostatically less stable south of the Polar Front.

(7) The nonlinear advection does not affect the general circulation pattern evidently, but does affect the formation of the mesoscale eddies, and especially the UB eddy (all seasons) and the JB gyre (spring).

(8) The model wind effects on the JES circulation are more pervasive than those of non-linear dynamic effects. The winter winds cause a strong basin-wide JES cyclonic gyre with 8 Sv recirculation in the northern JES and the summer winds drive a weak nearly basin-wide JES anticyclonic gyre. Thus, the wind forcing is the most important fact (80%) for the generation of the JB cyclonic gyre. The winds also influence the surface circulation such as driving the LC (winter), damping the EKWC (winter),

generating the UB eddy (all seasons), and generating eddies along the JCC (all seasons).

The wind has almost no effect on the occurrence of the JCC for all seasons.

(9) The model boundary-forcing enhances (weakens) the JES volume transport in the summer (winter). It has very weak effects on the occurrence of the LC except in the winter, when the boundary-forcing accounts for 30% of the LC at 46°N. It weakens the JB cyclonic gyre by 2 Sv (25%) in the winter. Besides, the boundary forcing also influences the surface circulation such as driving the UB eddy in all the seasons (50% in the winter), generating the EKWC (50-100% in the winter and 21% in the summer), and generating the JCC and eddies along the JCC.

(10) Future studies should concentrate on less simplistic scenarios. Realistic lateral transport should be included and the use of extrapolated climatological winds needs to be upgraded to incorporate synoptic winds to improve realism. Finally, the assumption of quasi-linearity that allowed us to use simple differences to quantify the effect of external forcing needs to be rigorously tested. It is important to develop a thorough methodology to perform sensitivity studies under the highly non-linear conditions that may exist in the littoral environment.

LIST OF REFERENCES

Betts, A. K., J. Ball, J. Beljaars, and C. M.Anton, 1996: The land surface-atmosphere interaction: A review based on observational and global modeling perspectives. *J. Geophys. Res.*, 101, 7209-7225.

Blumberg, A., and G. Mellor, 1987: A description of a three dimensional coastal ocean circulation model. Three-Dimensional Coastal Ocean Models, edited by N.S. Heaps, *American Geophysics Union*, Washington D.C., 1-16.

Chu, P.C., 1995: P-vector method for determining absolute velocity from hydrographic data. *Marine Tech. Soc. J.*, 29 (3), 3-14.

Chu, P.C., C.W. Fan, and W.J. Cai, 1998a: P-vector inverse method evaluated using the Modular Ocean Model (MOM). *J. Oceanogr.*, 54, 185-198.

Chu, P.C., S.H. Lu, and Y.C. Chen, 1998b: Wind-driven South China Sea deep basin warm-core /cool-core eddies, *J. Oceanogr.*, 54, 347-360.

Chu, P.C., Y.C. Chen, S.H. Lu, 1998c: Temporal and spatial variabilities of Japan Sea surface temperature and atmospheric forcings. *J. Oceanogr.*, 54, 273-284.

Chu, P.C., S.H. Lu, and Y.C. Chen, 1999a: A coastal atmosphere-ocean coupled system (CAOCS) evaluated by an airborne expandable bathythermograph survey in the South China Sea, May 1995. *J. Oceanogr.*, 55, 543-558.

Chu, P.C., N.L. Edmons, and C.W. Fan, 1999b: Dynamical mechanisms for the South China Sea seasonal circulation and thermohaline variabilities. *J. Phys. Oceanogr.*, in press.

Chu, P.C., and J. M. Veneziano, 1999c: Response of the South China Sea to tropical cyclone Ernie 1996. *J. Geophys. Res.*, in revision.

Chu, P.C., J. Lan, and C.W. Fan, 1999d: Japan/East Sea (JES) seasonal circulation and thermohaline variabilities. *J. Phys. Oceanogr.*, submitted.

Chu, P.C., S.H. Lu, and Y.C. Chen, 1999e: Circulation and thermohaline structures of the Japan/east Sea (JES) and adjacent seas simulated by a nested basin/coastal model, p 108-111, *Proceedings of the CREAMS'99 International Symposium*, Fukuoka, Japan, Jan. 26-28, 1999.

Chu P. C., Y. Chen, S. Lu, 1999f: Japan/East Sea (JES) Polar Front Meandering and Eddy Shedding in May 1995, pp. 11-13, *Proceedings of the CREAMS'99 International Symposium*, Fukuoka, Japan, Jan. 26-28, 1999.

Ezer, T. and G. Mellor, 1992: A numerical study of the variability and the separation of the Gulf Stream, induced by surface atmospheric forcing and lateral boundary flows. *J. Geophys. Res.*, 22, 660-682.

Guo, X., Y. M. H. Hukuda, T. Yamagata, 1999. Volume Transport through the Straits of Japan/East Seas - Preliminary Results from a Nested Ocean Model for Japan Coastal Ocean Predictability Experiment (JCOPE), pp. 140-143, *Proceedings of the CREAMS'99 International Symposium*, Fukuoka, Japan, Jan. 26-28, 1999.

Haney, R.L., 1971: Surface boundary conditions for ocean circulation models, *J. Phys. Oceanogr.*, 1, 241-248.

Hase, H., J.-H. Yoon, W. Koterayama, 1999. The Branching of the Tsushima Warm Current along the Japanese coast., p 19-22, *Proceedings of the CREAMS'99 International Symposium*, Fukuoka, Japan, Jan. 26-28, 1999.

Hellerman, S. and M. Rosenstein, 1983. Normal monthly wind stress over the world ocean with error estimates. *J. Phys. Oceanogr.*, 13, 1093-1104.

Hogan, P. J., H. E. Hurlburt, 1999. Impact of Different Wind Forcing on Japan/East Sea Circulation, p 124-127, *Proceedings of the CREAMS'99 International Symposium*, Fukuoka, Japan, Jan. 26-28, 1999.

Holloway, G.T. Sou and M. Eby, 1995. Dynamics of circulation of the Japan Sea. *J. Mar, Res.*, 53, 539-569.

Isoda, Y., 1994. Interannual SST variation to the north and south of the Polar front in the Japan Sea. *La Mer,* 32, 285-293.

Isoda, Y., S. Saitoh and M. Mihara, 1991. Sea surface temperature structure of the Polar front in the Japan Sea. *Oceanography of Asian Marginal Seas,* edited by K. Fakano, Elsevier, New York, 103-112.

Isoda, Y. and S. Saitoh, 1993. The northward intruding eddy along the east coast of Korea. *J. Oceanogr.*, 49, 443-458.

Kawabe, M., 1982a: Branching of the Tsushima Current in the Japan Sea, Part I: Data analysis. *J. Oceanogr. Soc.*, 38, 95 - 107.

Kawabe, M., 1982b: Branching of the Tsushima Current in the Japan Sea, Part II: Numerical experiment. *J. Oceanogr. Soc.*, 38, 183 - 192.

Kim, C.-H. and J.-H. Yoon, 1994: A numerical study on the seasonal variation of the Tsushima Warm Current along the coast of Japan. *Proceedings of the CREAMS Third Workshop*. Seoul, Korea, pp. 73-79.

Kim, C.-H., 1996: A numerical experiment study on the circulation of the Japan Sea (East Sea). Ph.D. thesis, Kyushu Univ., 151 pp.

Kim. C.-H. and J.-H. Yoon, 1996: Modeling of the wind-driven circulation in the Japan Sea using a reduced gravity model. *J. Oceanogr.*, 52, 359-373.

Levitus, S., 1982. *Climotological atlas of the World Ocean*. NOAA Prof. Paper 13, Washington D.C.

Mellor, G., 1992: Users guide for a three-dimensional, primitive equation, numerical ocean model. *Princeton University*, 34 pp.

Mellor, G., and T. Ezer, 1991: A Gulf Stream model and an altimetry assimilation scheme. *J. Geophys. Res.*, 96, 8779-8795.

Mellor, G., and T. Yamada, 1982: Development of a turbulence closure model for geophysical fluid problems. *Rev. Geophys. Space Phys.*, 20, 851-875.

Morimoto, T. Yanagi and A. Kaneko, 1999. Eddy Field in the Japan Sea Derived from Altimetric Data of TOPEX/POSEIDON and ERS-2, *Proceedings of the CREAMS'99 International Symposium*, Fukuoka, Japan, Jan. 26-28, 1999.

Mooers, C.N. K., H. Kang, S. Chen, 1999. Simulation of the Response of the Japan (East) Sea (JES) to Siberian Cold Air Outbreaks, 112-115, *Proceedings of the CREAMS'99 International Symposium*, hel in Fukuoka, Japan, Jan. 26-28, 1999.

Mooers, C. N.K. and H.-S. Kang (1995). Initial spin-up of a Sea of Japan numerical circulation model. In: (Eds. A.S. Alekseev and N.S. Bakhvalov) *Advanced Mathematics: Computations and Applications*, NCC Publisher, Novosibirsk; pp. 350-357.

Preller and Hogan, 1998. *The Sea*, 11, edited by Robinson and Brink, 429-482.

Ro, Y. J., 1999. Numerical Experiments of the Meso - Scale Eddy Activities in the East (Japan) Sea, p 116-119, *Proceedings of the CREAMS'99 International Symposium*, Fukuoka, Japan, Jan. 26-28, 1999.

Sekine, Y., 1991a. Wind-driven circulation in the Japan Sea and its influence on the branching of the Tsushima Current. *Prog. Oceanogr.*, 17, 297-312.

Sekine, Y., 1991b. A numerical experiment on the seasonal variation of the oceanic circulation in the Japan Sea. *Oceanography of Asian Marginal Seas* (Ed., K. Takano) Elsevier Oceanography Series, 54, 113-128.

Seo, J. W., 1998: Research on the sea surface winds and heat flux in the East Asian Marginal Seas. Ph.D. Thesis, Hanyang University.

Seung, Y.H. and K. Kim, 1989: On the possible role of local thermal forcing on the Japan Sea circulation. *J. Oceanol. Soc. Korea*, 24: 1-14.

Seung, Y.H., S.Y. Nam, and S.R. Lee, 1990: A combined effect of differential cooling and topography on the formation of Ulleung Warm Eddy. *Bull. Korean Fish. Soc*, 22, 375-384.

Seung, Y.-H. and S.-Y. Nam, 1991: Effect of winter cooling of subsurface hydrographic conditions off Korean Coast in the East (Japan) Sea. In: *Oceanography of Asian Marginal Seas* (Ed., K. Takano) Elsevier Oceanography Series, 163-178.

Seung, Y.H., 1992: A simple model for separation of East Korean Warm Current and formation of the North Korean Cold Current. *J. Oceanol. Soc. Korea*, 27, 189-196.

Seung, Y.H. and S.Y. Nam, 1992: A numerical study on the barotropic transport of the Tsushima Warm Current. *La mer*, 30, 139-147.

Seung, Y.H. and S.Y. Nam, 1992: A two-layer model for the effect of cold water formation on the East Korean Warm Current. *Bull. Korean Fish. Soc*, 25, 65-72.

Seung, Y.H. and K. Kim, 1993: A numerical modeling of the East Sea circulation. *J. Oceanol. Soc. Korea*, 28, 292-304.

Seung, Y.H. and K.J. Kim, 1995: A multilayer model for dynamics of upper and intermediate layer circulation of the East Sea. *J. Oceanol. Soc. Korea*, 30, 227-236.

Seung, Y. H. and J. H. Yoon, 1995. Some features of winter convection in the Japan Sea. *J. Oceanogr.*, 51, 61-73.

Takematsu, M., A.G. Ostrovski and T. Kitamura, 1994: Current features in the Japan Sea proper water. *Proc. of the Third CREAMS Workshop*, Seoul, Korea, 1-4.

Takematsu, M., H. Hase and Z. Nagano, 1996. Moored instrument observations in the Japan Sea Proper Water. In: *Proceedings of the Fourth CREAMS Workshop,* Vladivostok, 101-105.

Tomczak, M. and Godfrey, J. S., *Regional Oceanography: an Introduction,* 1t ed., Pergamon, 1994.

Toba et. Al, 1982. *La Mer*, 20, 41-51.

Uda, M., 1934. The results of simultaneous oceanographic investigation in the Japan Sea and its adjacent waters in May and June, 1932. *Journal of Imperial Fishery Experimental Stations,* 5, 57-190.

Watanabe, T., M. Hirai, J. H. Yoon, 1999: CTD Data Assimilation with an OGCM of the Japan Sea, p 148-151, *Proceedings of the CREAMS'99 International Symposium,* Fukuoka, Japan, Jan. 26-28, 1999.

Yoon, J.-H., 1982a: Numerical experiment on the circulation in the Japan Sea, Part I. Formation of the East Korean Warm Current. *J. Oceanogr. Soc. Japan*, 38, 43-51.

Yoon, J.-H. 1982b: Numerical experiment on the circulation in the Japan Sea, Part II. Influence of seasonal variations in atmospheric conditions on the Tsushima Current. *J. Oceanogr. Soc. Japan*, 38, 81-94.

Yoon, J.-H. 1982c: Numerical experiment on the circulation in the Japan Sea Part, III. Mechanism of the Nearshore Branch of the Tsushima Current. *J. Oceanogr. Soc. Japan*, 38, 125-130.

THIS PAGE INTENTIONALLY LEFT BLANK

INITIAL DISTRIBUTION LIST

1. Defense Technical Information Center 2
   8725 John J. Kingman Rd., STE 0944
   Ft. Belvoir, VA 22060-6218

2. Dudley Knox Library 2
   Naval Postgraduate School
   411 Dyer Rd.
   Monterey, CA 93943-5100

3. Chairman, Code OC/Bf 1
   Department of Oceanography
   Naval Postgraduate School
   Monterey, CA 93943-5100

4. Professor Peter C. Chu, Code OC 3
   Department of Oceanography
   Naval Postgraduate School
   Monterey, CA 93943-5100

5. Hilbert Strauhs 4
   Rua Rio Grande do Sul, 116 Ap. 114
   80620-080 Curitiba (PR)
   BRAZIL

6. Superintendent 1
   Naval Research Laboratory
   7 Grace Hopper Road
   Monterey, CA 93943-5502

7. Chairman 1
Oceanography Department
U.S. Naval Academy
Annapolis, MD 21402

8. Office of Naval Research (Code 420) 1
800 N. Quincy Street
Arlington, VA 22217

9. Dr. Martha Head 1
Naval Oceanographic Office
Stennis Space Center, MS 39522

10. Dr. Charles Horton 1
Naval Oceanographic Office
Stennis Space Center, MS 39522

11. Dr. Mike Carron 1
Naval Oceanographic Office
Stennis Space Center, MS 39522

12. NOAA Library 1
7600 Sand Point Way NE
Building 3
Seattle, WA 98115